Article

Neuron

IGF1-Dependent Synaptic Plasticity of Mitral Cells in Olfactory Memory during Social Learning

Highlights

- STFP induces a glomerulus-specific LTP at G-M synapse in the olfactory bulb
- This LTP requires Ca^{2+} sensor Syt10 that triggers IGF1 release from mitral cell
- IGF1 induces an IGF1R-dependent LTP by enhancing GABA-R function in mitral cell
- This socially relevant LTP is essential for memory encoding after STFP

Authors

Zhihui Liu, Zijun Chen, Congping Shang, ..., Dapeng Li, Thomas C. Südhof, Peng Cao

Correspondence

tcs1@stanford.edu (T.C.S.), caopeng@nibs.ac.cn (P.C.)

In Brief

Liu et al. demonstrate that mouse social learning induces a glomerulus-specific LTP at GABAergic G-M synapse in the olfactory bulb, revealing a synaptic substrate for a socially conditioned long-term memory that operates at the level of sensory information processing.

Liu et al., 2017, Neuron *95*, 106–122
July 5, 2017
http://dx.doi.org/10.1016/j.neuron.2017.06.015

CellPress

CellPress

Neuron
Article

IGF1-Dependent Synaptic Plasticity of Mitral Cells in Olfactory Memory during Social Learning

Zhihui Liu,[1,2,3] Zijun Chen,[1,4] Congping Shang,[1,4] Fei Yan,[1,4] Yingchao Shi,[1,4] Jiajing Zhang,[1] Baole Qu,[1,4] Hailin Han,[1] Yanying Wang,[1] Dapeng Li,[5] Thomas C. Südhof,[2,3,*] and Peng Cao[1,5,6,*]

[1]State Key Laboratory of Brain and Cognitive Sciences, CAS Center for Excellence in Biomacromolecules, Institute of Biophysics, Chinese Academy of Sciences, Beijing 100101, China
[2]Howard Hughes Medical Institute, Stanford University School of Medicine, Stanford, CA 94305, USA
[3]Department of Molecular and Cellular Physiology, Stanford University School of Medicine, Stanford, CA 94305, USA
[4]University of Chinese Academy of Sciences, Beijing 100049, China
[5]National Institute of Biological Sciences, Beijing 102206, China
[6]Lead Contact
*Correspondence: tcs1@stanford.edu (T.C.S.), caopeng@nibs.ac.cn (P.C.)
http://dx.doi.org/10.1016/j.neuron.2017.06.015

SUMMARY

During social transmission of food preference (STFP), mice form long-term memory of food odors presented by a social partner. How does the brain associate a social context with odor signals to promote memory encoding? Here we show that odor exposure during STFP, but not unconditioned odor exposure, induces glomerulus-specific long-term potentiation (LTP) of synaptic strength selectively at the GABAergic component of dendrodendritic synapses of granule and mitral cells in the olfactory bulb. Conditional deletion of synaptotagmin-10, the Ca^{2+} sensor for IGF1 secretion from mitral cells, or deletion of IGF1 receptor in the olfactory bulb prevented the socially relevant GABAergic LTP and impaired memory formation after STFP. Conversely, the addition of IGF1 to acute olfactory bulb slices elicited the GABAergic LTP in mitral cells by enhancing postsynaptic GABA receptor responses. Thus, our data reveal a synaptic substrate for a socially conditioned long-term memory that operates at the level of the initial processing of sensory information.

INTRODUCTION

Learning from conspecifics is prevalent among social animals (Gariépy et al., 2014). For example, after only a single trial of olfactory social learning, rodents form long-term memories of their mates, territories, and safe foods, all of which are essential for survival (Galef, 1982; Brennan et al., 1990; Lesburguères et al., 2011). Social context, consisting of a diverse repertoire of socially relevant chemical and physical signals, plays a fundamental role in these behavioral paradigms.

How the brain associates social context with sensory stimuli to encode memory during social learning is a long-standing and unresolved question. Two series of seminal studies provide important clues. First, Keverne and colleagues (Brennan et al., 1990; Keverne and Brennan, 1996) demonstrated that pheromone-dependent social recognition memory is associated with a potentiation of GABAergic feedback inhibition between granule and mitral cells in mouse accessory olfactory bulb. However, the nature of the synaptic changes that were observed remained unclear, as did the underlying molecular mechanisms and behavioral relevance of these changes. Second, socially acquired food preference depends on the association of food odors with semiochemicals (e.g., carbon disulfide) in the main olfactory bulb (MOB) of rodents (Galef et al., 1988; Munger et al., 2010), but the synaptic substrate for such association was not identified yet. These two observations suggest that the neural substrate for association of sensory cues with social context in rodent brain may exist in the olfactory system.

In the main olfactory system of vertebrates, odor information is sequentially processed in the main olfactory epithelium (MOE) and the MOB. In the MOE, each olfactory sensory neuron (OSN) expresses one particular odorant receptor that can detect a limited number of odorants at physiological concentrations (Buck and Axel, 1991; Serizawa et al., 2003). Axons from the OSNs that express the same odorant receptor converge onto one or two glomerluli in each MOB, forming a two-dimensional olfactory sensory map (Ressler et al., 1994; Mombaerts et al., 1996; Vincis et al., 2012). In the MOB, the glomerular layer (GL) and the external plexiform layer (EPL) represent two major stations for olfactory information processing (Uchida et al., 2014). In the GL, OSNs provide excitatory input to the primary dendrites of 20–50 mitral/tufted (M/T) cells, the major output neurons of the MOB (Shepherd et al., 2004). Notably, olfactory signals are not simply relayed from OSNs to M/T cells, but they are processed in the glomeruli by a complex neuronal network formed by periglomerular (PG) neurons, OSNs, and M/T cells (De Saint Jan et al., 2009; Najac et al., 2011; Gire et al., 2012; Shao et al., 2012; Vaaga and Westbrook, 2016; Bourne and Schoppa, 2017). In the EPL, the lateral dendrites of M/T cells elaborate dendrodendritic synapses with inhibitory interneurons, such as granule cells (Shepherd et al., 2007) and parvalbumin-positive (PV^+) interneurons (Kato et al., 2013; Miyamichi et al., 2013). Dendrodendritic synapses between M/T cells and granule cells are reciprocal; the lateral dendrite of an M/T cell forms an excitatory synapse on the dendrite of a granule cell, which then forms

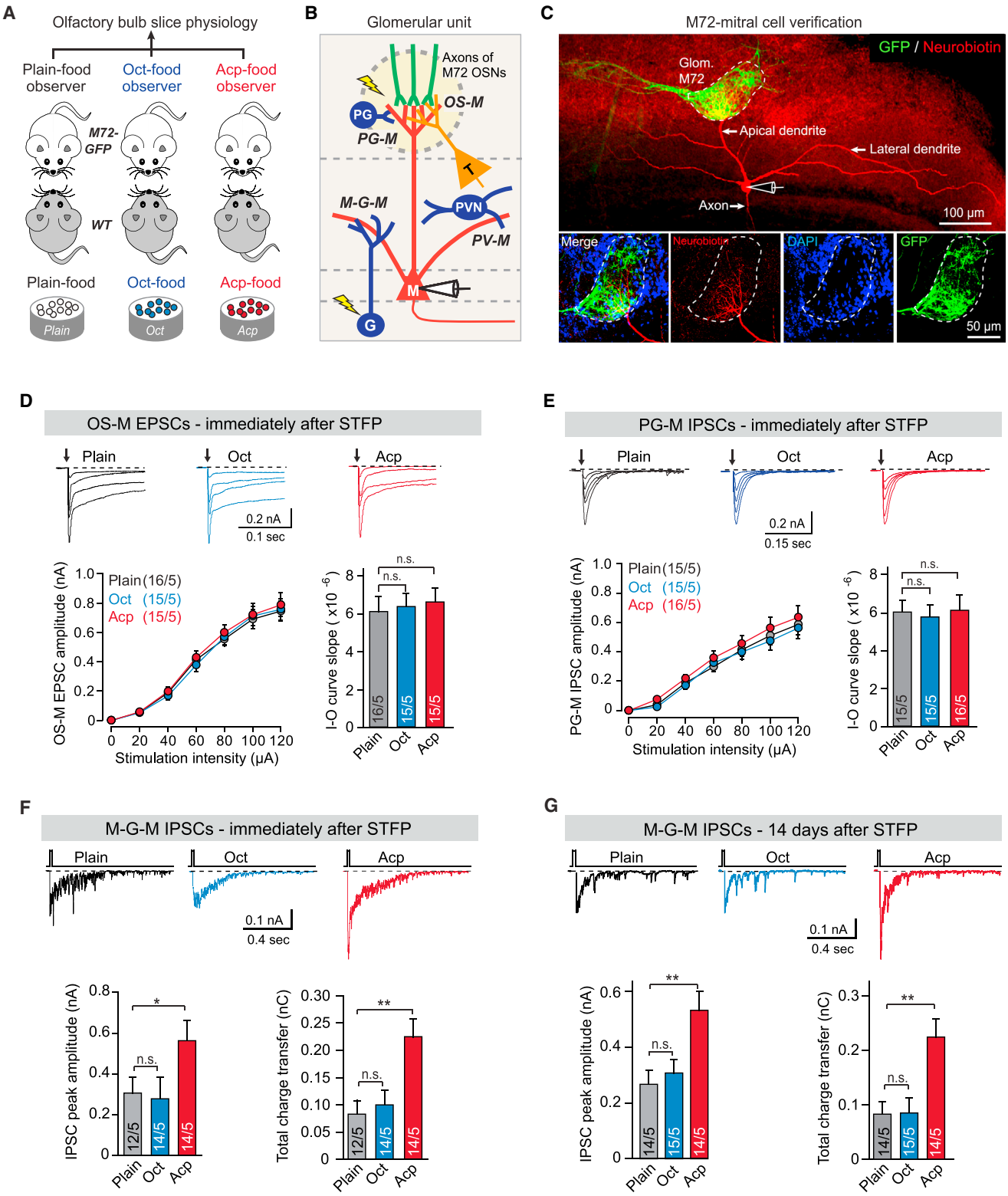

Figure 1. STFP Learning Induces an Odor-Specific Type of LTP

(A) *M72-GFP* mice received STFP training and were subjected to slice physiology.

(B) Schematic diagram showing the major local synaptic inputs to mitral cells in M72 glomerular unit. M, mitral cells; G, granule cells; PVN, PV^{+} interneurons; PG, periglomerular cells; OSN, olfactory sensory neurons; T, external tufted cells.

(legend continued on next page)

an inhibitory synapse onto the lateral dendrite of the M/T cell in an immediate feedback loop (Jahr and Nicoll, 1980; Isaacson and Strowbridge, 1998; Schoppa et al., 1998; Chen et al., 2000; Shepherd et al., 2007).

An important feature of the multi-layered microcircuits in the MOB is their modular organization. Evidence from morphological, functional, and modeling studies suggests that intrabulbar neurons are clustered to form glomerular units (Stewart et al., 1979; Kauer and Cinelli, 1993; Willhite et al., 2006; Migliore et al., 2015). The different types of neurons associated with the same glomerular unit share similar profiles of olfactory tuning with varied tuning sharpness and spike timing (Tan et al., 2010; Dhawale et al., 2010; Kikuta et al., 2013). Such modular organization of microcircuits in the MOB provides an opportunity to identify glomerulus-specific mechanisms underlying social learning.

Here we used social transmission of food preference (STFP) as a social learning paradigm (Galef, 2003; Wrenn, 2004) to study the synaptic mechanism for the association of sensory cues with social context in the MOB. We found that STFP induced a significant, long-lasting, and selective strengthening, referred to as long-term potentiation (LTP), of reciprocal synapses between granule and mitral cells associated with the glomerular unit sensitive to the memorized odors. Strikingly, odor exposure without a social context did not induce this LTP. This LTP required activity-dependent IGF1 signaling and was essential for memory formation. Thus, our data reveal a synaptic substrate that associates social context with sensory cues for memory encoding during social learning.

RESULTS

Monitoring Diverse Mitral Cell Synapses in Acute MOB Slices

To analyze synapses of mitral cells associated with a specific glomerular unit, we used gene-targeted *M72-GFP* mice in which M72 glomeruli innervated by axon terminals of GFP^+ M72 OSNs are fluorescently labeled (Potter et al., 2001). M72 OSNs are sensitive to acetophenone (Acp) but insensitive to octanal (Oct) (Zhang et al., 2012). During STFP training, *M72-GFP* observer mice interacted with demonstrator mice that had ingested plain food, Acp-flavored food, or Oct-flavored food (both at 1%). We then prepared acute MOB slices (300 μm) from the M72-GFP observer mice immediately or 14 days after STFP training, and we performed whole-cell recordings from M72-associated mitral cells (Figure 1A). In parallel behavioral experiments, we confirmed that the mice had formed a long-term memory of the food odor after STFP training (Figures S1A–S1C).

In our experiments, we routinely analyzed three types of synapses formed on M72-associated mitral cells: (1) excitatory synapses formed by M72 OSNs (OS-M synapses), (2) inhibitory synapses formed by PG neurons in the local neuronal network of the M72 glomerulus (PG-M synapses), and (3) dendrodendritic reciprocal synapses formed by mitral and granule cells (M-G-M synapses) (Figure 1B). For studying excitatory OS-M and inhibitory PG-M synapses, we delivered low-frequency (0.067 Hz) stimulation with a bipolar electrode placed adjacent to the GFP^+ M72 glomerulus, and we recorded excitatory postsynaptic currents (EPSCs) (with picrotoxin in the artificial cerebrospinal fluid [ACSF]) and inhibitory postsynaptic currents (IPSCs) (with D-(-)-2-amino-5-phosphonopentanoic acid [D-AP5] and 6-cyano-7-nitroquinoxaline-2,3-dione [CNQX] in the ACSF) from M72-associated mitral cells (Figures S1D–S1H; Vaaga and Westbrook, 2016). For examining M-G-M synapses, we recorded recurrent IPSCs from M72-associated mitral cells in the absence of receptor antagonists, using the same patch-clamp pipette for stimulations (10-ms membrane depolarization from −70 to 0 mV) and recordings (Figures S2A and S2B; Isaacson and Strowbridge, 1998; Schoppa et al., 1998; Chen et al., 2000). In addition, we separately monitored the inhibitory G-M and excitatory M-G sub-synapses of the M-G-M dendrodendritic synapses. Using bipolar stimulation electrodes placed in the granule cell layer, we recorded G-M IPSCs from M72-associated mitral cells in the presence of D-AP5 and CNQX (Figures S2F–S2H) and M-G EPSCs from granule cells in the presence of picrotoxin (Figures S2I and S2J). Finally, in selected experiments we also recorded M72-associated mitral cell IPSCs that were evoked by optogenetic activation of PV^+ interneurons expressing ChR2-EYFP (Figures S2C–S2E; Kato et al., 2013; Miyamichi et al., 2013).

Several concerns about the specificity of these recordings may be raised. First, are we faithfully recording from mitral cells associated with GFP^+ M72 glomeruli? In *M72-GFP* mice, ~20–50 mitral cells innervate each of the four GFP^+ M72 glomeruli (Tan et al., 2010; Dhawale et al., 2010; Kikuta et al., 2013), thus ensuring that most mitral neurons in the vicinity of a glomerulus actually innervate that glomerulus. Nevertheless, to ensure that patched mitral cells were associated with the M72 glomerulus, we verified this association by neurobiotin injections and histology after recordings (Tan et al., 2010). Only mitral cells with fluorescent primary dendrites innervating the GFP^+ M72 glomerulus (Figure 1C) were included in the analyses.

Second, quantification of synaptic responses induced by extracellular stimulation in slices is difficult since the number of stimulated synapses cannot be controlled. Therefore, we based our measurements of synaptic strength on input/output curves,

(C) Example micrograph showing histological verification of a recorded M72-associated mitral cell (red) with the primary dendrite projecting to the GFP^+ M72 glomerulus (green).

(D and E) Example traces (top), with summarized input-output curves and curve slopes (bottom) of OS-M EPSCs (D) or PG-M IPSCs (E) from M72-associated mitral cells of *M72-GFP* observer mice immediately after STFP training.

(F and G) Example traces (top), with summarized peak amplitude and charge transfer (bottom) of M-G-M IPSCs evoked by brief membrane depolarization (10 ms) from M72-associated mitral cells immediately (F) and 14 days (G) after STFP training. For more OS-M EPSC, PG-M IPSC, M-G-M IPSC, and PV-M IPSC data, see Figures S1 and S2.

Data in (D)–(G) are means ± SEM (error bars), with mouse number as sample size n; numbers of neurons/mice are indicated in bars. Statistical analysis is by Student's t test (*$p < 0.05$ and **$p < 0.01$; n.s., $p > 0.1$).

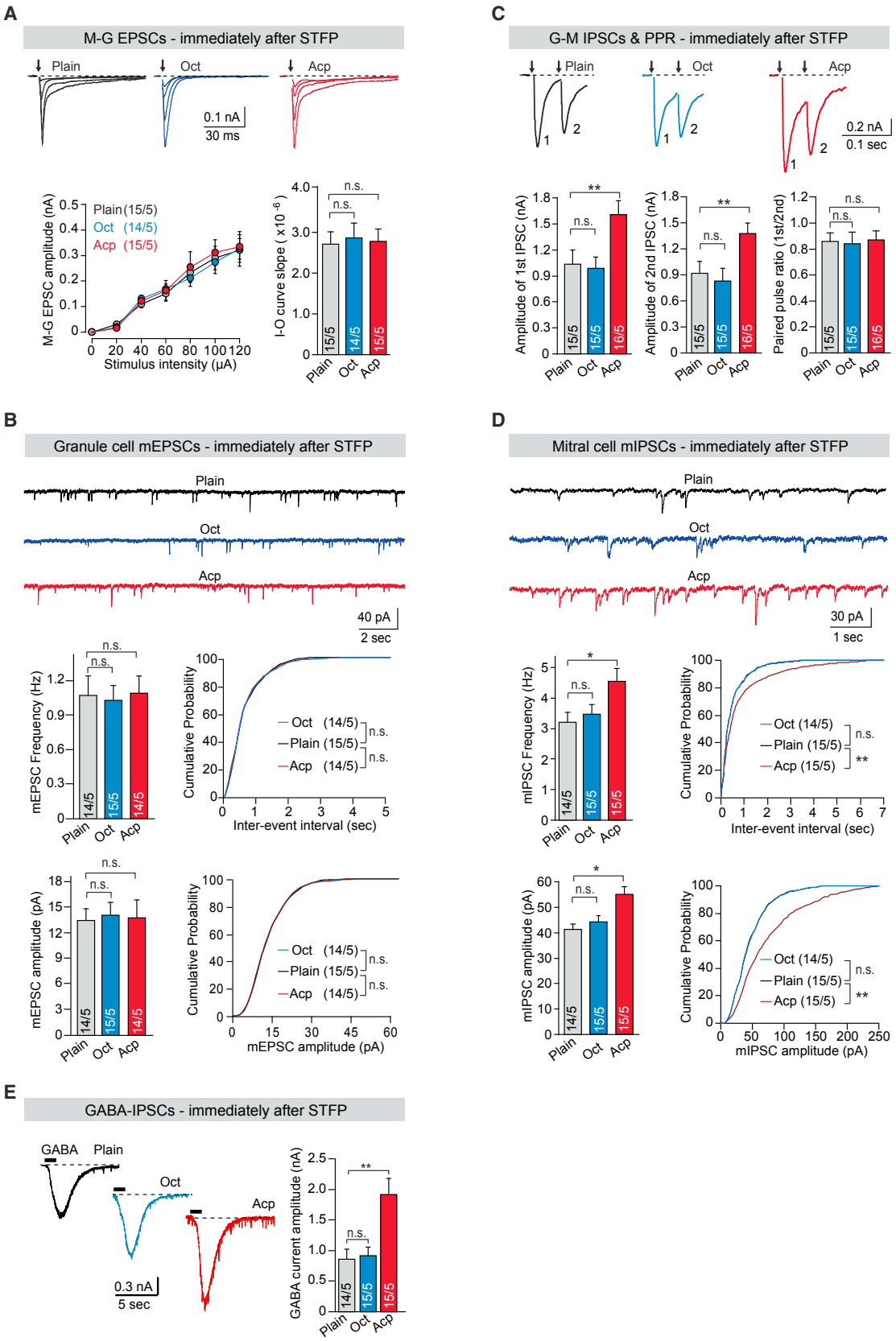

(legend on next page)

and we calculated synaptic strength as the slope of the input/output curve. Moreover, we used as controls slices from naive mice and from mice exposed to Oct, which is not an M72 ligand; the fact that the synaptic strength of these two controls was similar under all conditions validates the measurements (see below in Figures 1D–1G).

Third, do our recordings actually monitor the intended synapses? Considering the combination of electrode placements with pharmacological antagonists, this seems likely. However, it should be noted that, given the complex neuronal network in olfactory glomeruli, the measured synaptic responses for OS-M and PG-M synapses are probably not exclusively monosynaptic (De Saint Jan et al., 2009; Najac et al., 2011; Gire et al., 2012; Shao et al., 2012; Vaaga and Westbrook, 2016; Bourne and Schoppa, 2017). Indeed, we found that OS-M EPSCs exhibited a complex waveform (Figure S1F), consisting of a transient mono-synaptic phase (latency to peak: 4.2 ± 0.2 ms) followed by a long-lasting decay phase (decay-to-baseline time: 1.35 ± 0.3 s; Figures S1I–S1K). This broad waveform likely arises because OSNs form direct excitatory contacts with the dendrites of both mitral and external tufted cells, with the dendrites additionally connected by gap junctions (Vaaga and Westbrook, 2016; Bourne and Schoppa, 2017). Thus, although we refer to OS-M and PG-M synapses, we mean to imply with this term that the respective synaptic responses reflect the overall synaptic strength of the OSN/mitral cell and the PG neuron/mitral cell connections, and not necessarily a simple mono-synaptic connection. Since STFP induces no changes in these synapses and these synapses serve as controls for the changes we observed in M-G-M synapses (see below in Figures 1D and 1E), the precise nature of OS-M EPSCs and PG-M IPSCs is not of primary importance for the present study.

STFP Selectively Induces LTP at M-G-M Reciprocal Synapses

We observed no STFP-induced changes in the strength of OS-M (Figure 1D), PG-M (Figure 1E), or PV-M synapses (Figure S2E) in M72-associated mitral cells in mice that were exposed to plain food or to Acp- or Oct-flavored food. However, we found that STFP with Acp-flavored food strongly potentiated reciprocal M-G-M synapses, measured by mitral cell recurrent inhibition (Isaacson and Strowbridge, 1998; Schoppa et al., 1998; Chen et al., 2000; Figure 1F). As a control, we detected no changes in M-G-M synapses after STFP with Oct-flavored or plain food, and we found that recurrent inhibition of mitral cells not associated with M72 glomeruli was not potentiated by STFP with Acp-flavored food (Figures S3A–S3C). The selective strengthening of M-G-M synapses of M72-associated mitral cells was fully maintained for at least 14 days (Figure 1G), suggesting that it represented LTP.

What is the nature of STFP-induced LTP at reciprocal M-G-M synapses? To address this question, we examined the effect of STFP on EPSCs in granule cells evoked by the stimulation of M72-associated mitral cells (M-G EPSCs; Figures 2A, S2I, and S2J) and on miniature EPSCs in these granule cells (mEPSCs; Figure 2B). We found no STFP-induced changes, thus excluding an enhancement of the M-G sub-synapse of reciprocal dendro-dendritic M-G-M synapses as a cause of the LTP. We then recorded IPSCs from M72-associated mitral cells evoked by granule cell stimulation (G-M IPSCs). We observed that STFP significantly increased the G-M IPSC amplitude in mitral cells, but it did not change the IPSC paired-pulse ratio (Figures 2C and S2F–S2H), suggesting a postsynaptic LTP at G-M synapses. In parallel experiments, we found that LTP of G-M synapses was not induced by simply exposing *M72-GFP* mice to Acp-flavored food on a filter paper outside the context of STFP (Figures S3D and S3E), indicating that LTP at G-M synapses requires a social context.

We also performed similar experiments with *M71-GFP* mice, which possess GFP^+ M71 glomeruli that are also sensitive to Acp and insensitive to Oct (Bozza et al., 2002). We found that STFP training with Acp-flavored food also induced LTP in G-M synapses of M71-associated mitral cells (Figures S3F–S3H). Thus, this LTP is a general feature and not specific to a particular line of genetically manipulated mice.

To further characterize the STFP-induced GABAergic LTP, we monitored in M72-associated mitral cells miniature IPSCs (mIPSCs), which are primarily mediated by G-M synapses owing to their high abundance. Strikingly, Acp-induced STFP significantly increased the mIPSC amplitude and frequency in M72-associated mitral cells (Figure 2D), suggesting that the synaptic changes during LTP were due to an increased postsynaptic GABA receptor (GABA-R) response. To test this hypothesis, we recorded inhibitory currents that were directly evoked in mitral cells by exogenously applied GABA (100 μM; Figures S2K and S2L). We detected a massive STFP-induced increase (>100%) in GABA-induced currents, confirming that STFP-induced LTP involves an increase in postsynaptic GABA-R response (Figure 2E). Together, these data suggest via multiple lines of evidence that STFP selectively causes an LTP of

Figure 2. Characterization of STFP-Induced LTP at M-G-M Reciprocal Synapses

(A) Example traces (top), with summarized input-output curves and curve slopes (bottom) of M-G EPSCs from granule cells associated with M72 mitral cells in *M72-GFP* observer mice immediately after STFP training.

(B) Example traces (top), with averaged frequency and cumulative probability of inter-event interval (middle), and averaged amplitude and cumulative probability of mEPSC amplitude (bottom) of granule cells associated with M72 mitral cells immediately after STFP training.

(C) Example traces (top), with summarized analyses of amplitude and ratio (bottom) of G-M IPSCs evoked by paired-pulse stimuli (120 μA) from M72-associated mitral cells immediately after STFP training.

(D) Example traces (top), with averaged frequency and cumulative probability of inter-event interval (middle), and averaged amplitude and cumulative probability of mIPSC amplitude (bottom) of M72-associated mitral cells immediately after STFP training.

(E) Example traces (left), with summarized amplitude of GABA current induced by the application of GABA (100 μM) to M72-associated mitral cells immediately after STFP training. For more data on M-G EPSCs, G-M IPSCs, and GABA IPSCs, see Figure S2.

Data of bar graphs in (A)–(E) are means ± SEM (error bars), with mouse number as sample size n; numbers of neurons/mice are indicated in bars. Statistical analysis is by Student's t test (*$p < 0.05$ and **$p < 0.01$; n.s., $p > 0.1$). Data of cumulative probability curves in (B) and (D) are analyzed by Kolmogorov-Smirnov test.

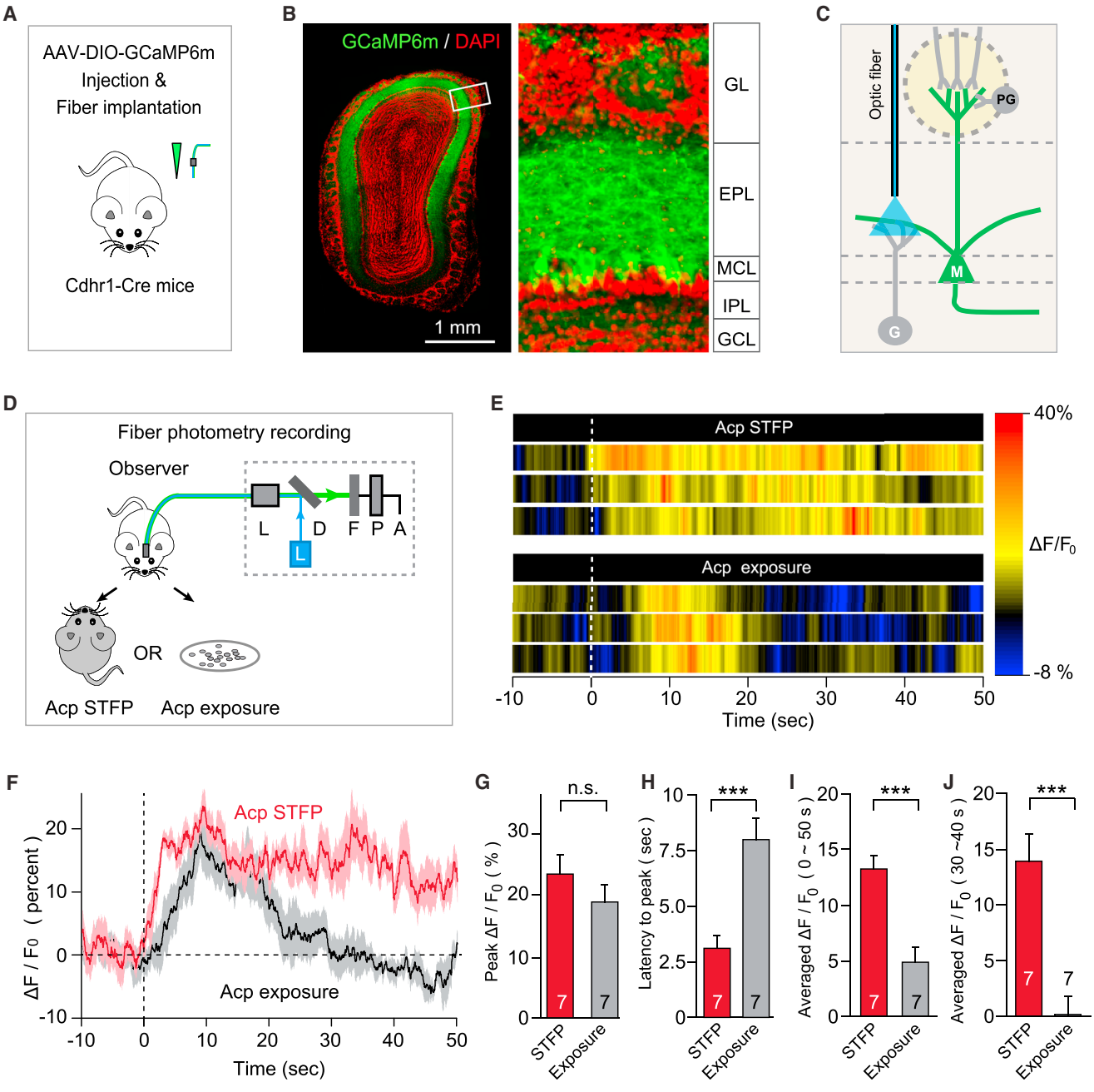

Figure 3. STFP Induces a Prolonged Ca^{2+} Wave in Dendrites of Mitral Cells in the MOB

(A) Schematic diagram showing stereotaxic injection of AAV-DIO-GCaMP6m and subsequent fiber implantation into the MOB of *Cdhr1-Cre* mice. Note the images were assembled with smaller imaging fields.

(B) Example MOB section (left) and cropped region (right) showing the selective expression of GCaMP6m (green) in mitral cells and their dendrites in the EPL of MOB.

(C and D) Schematic diagrams showing optic fiber implanted in the EPL to monitor GCaMP6m signals from mitral cell dendrites (C), while the freely moving mouse is subjected to STFP training or exposure to Acp-flavored food on a filter paper without a social context (D). See details of fiber photometry system in the STAR Methods.

(E) Example heatmap traces illustrating the time courses of Ca^{2+} signals from the same mitral cell dendrites in response to Acp STFP training (top) or exposure to Acp-flavored food (bottom). The dashed line indicates the time point to introduce the demonstrator or Acp-flavored food to the observer mice.

(F) Averaged traces of Ca^{2+} transients from seven Cdhr1-Cre mice before and during STFP training (red) or exposure to Acp-flavored food without a social context (black). Solid lines indicate mean and shaded areas indicate SEM. STFP evoked a prolonged Ca^{2+} wave consisting of repetitive Ca^{2+} transients, whereas Acp exposure alone induced a brief Ca^{2+} transient that decayed rapidly.

(legend continued on next page)

inhibitory responses in reciprocal M-G-M synapses of those mitral cells that are associated with glomeruli sensitive to the STFP odor. Since only the inhibitory G-M component, but not the excitatory M-G component, of the reciprocal M-G-M synapses was potentiated by STFP, we focused all subsequent experiments on G-M sub-synapses.

STFP Is Associated In Vivo with Long-Lasting Ca^{2+} Transients in Lateral Dendrites of Mitral Cells

To understand how STFP induces LTP in dendrodendritic G-M synapses, we monitored Ca^{2+} transients in mitral cell dendrites in vivo. We expressed GCaMP6m in mitral cells by injecting AAV-DIO-GCaMP6m into the MOB of *Cdhr1-Cre* mice (which express Cre-recombinase only in mitral cells; Wachowiak et al., 2013; Figures 3A and 3B). Three weeks after injections, we monitored Ca^{2+} transients in the lateral dendrites of mitral cells with an optic fiber implanted in the external plexiform layer close to the rostral M72 glomerulus (bregma 4.50 mm, lateral ±1.30 mm; Figure 3C). The freely moving mice with implanted optic fiber were subjected either to social interaction with demonstrators that ingested Acp-flavored food (Acp STFP) or to exposure to Acp-flavored food on a filter paper in the absence of a social context (Acp exposure; Figure 3D). Acp STFP elicited a rapid (latency to peak: 3.1 ± 0.6 s) and sustained (decay to baseline: 86.7 ± 26.9 s) Ca^{2+} wave consisting of a series of repetitive Ca^{2+} transients in mitral cell dendrites (example traces in Figure 3E; averaged data in Figures 3F–3J). By contrast, slower (latency to peak: 8.0 ± 0.9 s) and brief (decay to baseline: 28.6 ± 7.4 s) Ca^{2+} transients with a similar peak amplitude were elicited by Acp exposure without a demonstrator (Figures 3E–3J). Thus, odor exposure in a social context that induces LTP at G-M synapses elicited rapid and sustained Ca^{2+} transients in the lateral dendrites of mitral cells. Odor exposure without a social context that fails to induce this LTP (Figures S3D and S3E) elicited slow and brief Ca^{2+} transients.

The sustained and rapidly initiated GCaMP6m signal could reflect differences in how the mouse behaves while sampling odor under these two conditions. We examined the sniffing behavior of mice during odor exposure with and without a social context. The sniffing frequency and amplitude were significantly increased immediately after mice started odor sampling both with and without a social context (Figures S3I and S3J). However, the sniffing frequency and amplitude with a social context were not significantly different from those without a social context (Figures S3K and S3L), suggesting the difference of GCaMP6m signals is due to a central mechanism. Note, however, that these data do not reveal whether the in vivo Ca^{2+} transients actually trigger the LTP of G-M synapses. They only suggest that STFP-induced LTP at G-M synapses is mediated by an unidentified Ca^{2+}-signaling pathway in the lateral dendrites of mitral cells.

STFP-Induced LTP at G-M Synapses Is Mediated by Activity-Dependent IGF1 Signaling

How does Ca^{2+} trigger STFP-dependent LTP at G-M synapses? We hypothesized that Ca^{2+} may induce LTP by stimulating exocytosis of neurotransmitters or other signaling molecules. To explore this hypothesis, we tested the roles of two synaptotagmins, Syt1 and Syt10, which serve as Ca^{2+} sensors for exocytosis (Südhof, 2013). Knockdown (KD) of Syt1 as the dominant Ca^{2+} sensor for fast neurotransmitter release blocks fast synaptic transmission; thus, the Syt1 KD is a useful tool for testing the importance of fast synaptic transmission (Xu et al., 2012). Conditional knockout (cKO) of Syt10, conversely, has no effect on basal synaptic transmission, but it blocks activity-dependent IGF1 secretion from MOB neurons, allowing selective tests of the role of Ca^{2+}-triggered IGF1 exocytosis in LTP induction (Cao et al., 2011).

Immunohistochemistry of MOB sections revealed that Syt1 (Figures 4A, 4B, and S4) and Syt10 (Figures 4C, 4D, and S5) are abundantly expressed in the external plexiform layer that contains dendrodendritic M-G-M synapses. Approximately half of the presynaptic dendritic terminals of mitral cells, identified by vGlut1 staining, were positive for Syt10 (47% ± 11%, n = 3 mice; Figures 4E, 4F, and S5), suggesting that a considerable proportion of Syt10-containing vesicles that mediate IGF1 exocytosis in mitral cells are in close proximity to reciprocal M-G-M synapses.

To ablate Syt1 in vivo, we stereotaxically injected adeno-associated viruses (AAVs) encoding Syt1 small hairpin RNAs (shRNAs) and EGFP into the MOB of 2-month-old *M72-GFP* mice, with AAVs expressing EGFP as a control (Figures S6A–S6E). To delete Syt10, we injected AAVs encoding EGFP-tagged Cre-recombinase into the MOB of homozygous *Syt10 cKO* ($Syt10^{f/f}$) mice that had been crossed with *M72-GFP* mice, with AAVs encoding inactive Cre-recombinase as a control (Figures S6F–S6H). Using slice physiology, we found that the Syt1 KD in the MOB dramatically impaired basal synaptic transmission in G-M synapses as expected (Figure 4G). In contrast, the Syt10 KO had no effect on basal transmission at G-M synapses (Figure 4H), consistent with previous observations indicating that Syt10 is not a Ca^{2+} sensor for neurotransmitter release (Cao et al., 2011).

We next asked whether the Syt10 KO in the MOB impaired STFP-induced LTP at G-M synapses. We again injected AAVs encoding active or inactive (as control) Cre-recombinase bilaterally into the MOB of $Syt10^{f/f}$ mice that had been crossed with *M72-GFP* mice, and we subjected the mice to STFP training with demonstrators of plain, Acp-flavored, or Oct-flavored food (Figure 4I). Using slice recordings, we found that the Syt10 KO had no effect on synaptic strength at G-M synapses of M72-associated mitral cells after STFP with plain food or with Oct-flavored food (both of which did not induce LTP at these

(G and H) Comparisons of peak $\Delta F/F_0$ (G) and latency to reach peak (H) for Ca^{2+} signals induced by Acp STFP training and exposure to Acp without a social context.

(I and J) Comparisons of averaged Ca^{2+} signals ($\Delta F/F_0$) induced by STFP training and by exposure to Acp during the first 50 s (I) and during a late phase between 30 and 40 s after initiation (J).

Data in (F)–(I) are means ± SEM (error bars), with mouse number as sample size n; numbers of mice are indicated in bars. Statistical analysis is by Student's t test (n.s., $p > 0.1$; ***$p < 0.001$).

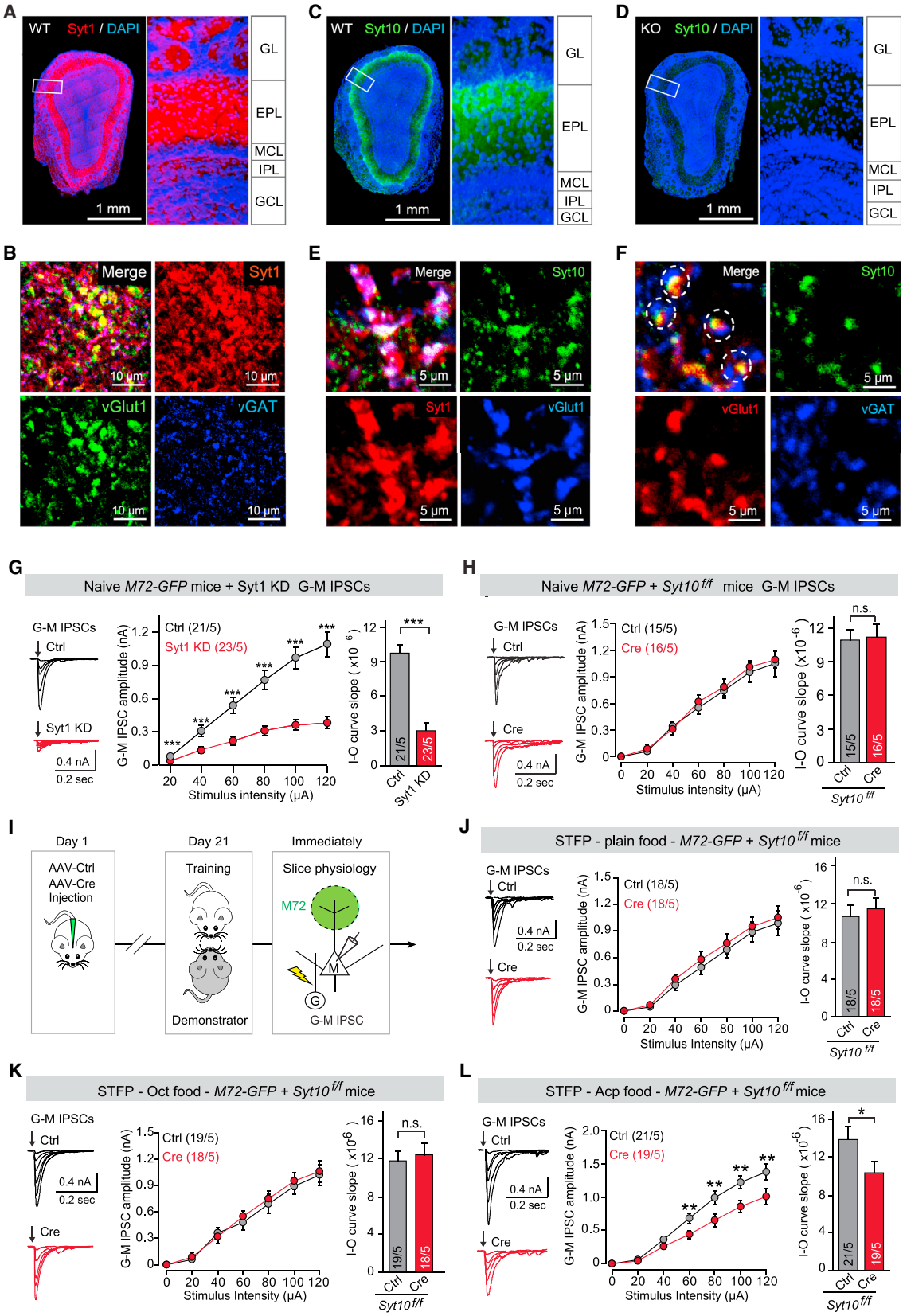

(legend on next page)

synapses; Figures 4J and 4K), but that the Syt10 KO blocked the STFP-induced LTP that is sensitive to Acp at G-M synapses of M72-associated mitral cells (Figure 4L).

Since the Syt10 KO ablates activity-dependent IGF1 secretion (Cao et al., 2011), we next tested whether IGF1 could be involved in the STFP-induced LTP at G-M synapses. IGF1 is synthesized in mitral cells (Bartlett et al., 1991) and acts as a neurotrophic factor to support intrabulbar neurogenesis and differentiation (Scolnick et al., 2008), but it has not previously been linked to long-term synaptic plasticity in the MOB. Thus, a plausible hypothesis to account for the role of Syt10 in STFP-induced LTP at G-M synapses is that social interaction-dependent long-lasting Ca^{2+} transients during STFP trigger Syt10-dependent IGF1 exocytosis (Cao et al., 2011), and the secreted IGF1 then induces G-M synaptic LTP.

To test this hypothesis, we examined whether IGF1 directly increases the strength of G-M synapses. We measured the effect of IGF1 on the amplitudes of G-M IPSCs and OS-M EPSCs (as a control) in mitral cells in acute MOB slices from wild-type mice. Application of IGF1 to acute slices did not alter OS-M EPSCs (Figures 5A–5C), but it caused a rapid and sustained potentiation of G-M IPSCs (Figures 5D–5F) that persisted during IGF1 treatment and lasted for at least 30 min after IGF1 wash-out (Figures S7A–S7D). The IGF1-induced potentiation of G-M IPSCs was blocked by the IGF1 receptor (IGF1-R) antagonist NVP-AEW541 (Figures 5D–5F), indicating that the synaptic potentiation was specifically caused by IGF1. The IGF1-induced increase in the strength of G-M synapses was associated with a concurrent increase in the amplitude (~30%) and frequency (~15%) of mIPSCs (Figures 5G and 5H), but not with a change in paired-pulse ratio (Figures 5I and 5J), again indicating that the effect of IGF1 is mediated by a postsynaptic mechanism.

IGF1 acts via binding to the IGF1-R and/or insulin receptor (Fernandez and Torres-Alemán, 2012). Both receptors are abundantly, but not exclusively, expressed in mitral cells of the MOB (Marks et al., 1991). We ablated the IGF1-R or insulin receptor by injecting AAVs expressing Cre-recombinase into the MOB of adult *IGF1-R*$^{f/f}$ or *insulin receptor*$^{f/f}$ mice (Brüning et al., 1998; Dietrich et al., 2000), and we tested the effect of IGF1 in acute slices from both mutant mice. We found that the insulin receptor KO had no effect on the IGF1-induced potentiation at G-M synapses, but that the IGF1-R KO blocked this synaptic potentiation (Figures 5K–5M). Thus, IGF1-induced synaptic potentiation is mediated by the IGF1-R that is expressed in mitral cells, suggesting an autocrine mechanism.

We examined the effects of postsynaptic membrane depolarization on mitral cell mIPSCs in acute olfactory bulb slices. Twenty postsynaptic depolarization pulses (from −70 to 10 mV for 1 s, separated by 6 s) were applied to mitral cells clamped at −70 mV with different combinations of D-AP5, CNQX, and tetrodotoxin (TTX) included in the ACSF (Kato et al., 2009). Postsynaptic depolarization only transiently increased mIPSC frequency and amplitude, without significant potentiation of mIPSC frequency and amplitude 28–30 min after depolarization (Figures S7E–S7I). Thus, direct depolarization of the postsynaptic neuron did not elicit LTP of GABAergic G-M synapses, consistent with an indirect effect of Ca^{2+} transients via activation of IGF1 exocytosis.

Up to this point, our results suggested that STFP induces activity-dependent secretion of IGF1 from mitral cells, which in turn induces an odor-specific LTP at G-M synapses in the MOB. To further test this hypothesis, we virally expressed active or inactive (as control) Cre-recombinase bilaterally in the MOB of adult *IGF1-R*$^{f/f}$ mice that had been crossed with *M72-GFP* mice, resulting in intrabulbar IGF1-R deletion in adult mice (Figure S6I). Recordings of basal synaptic transmission in acute slices revealed that, similar to the Syt10 deletion, the IGF1-R deletion had no effect on basal G-M synaptic transmission (Figure S6J). We then measured the effect of the IGF1-R KO on the STFP-induced LTP at G-M synapses of M72-associated mitral cells (Figure 6A). Again, similar to the Syt10 deletion, the IGF1-R KO selectively blocked LTP at these synapses after STFP with Acp food demonstrator (Figure 6D), but not after STFP with plain or Oct food demonstrators (Figures 6B and 6C). Viewed together, these data strongly suggest that IGF1-R signaling mediates STFP-induced LTP at G-M synapses in the MOB.

STFP-Induced LTP in G-M Synapses Is Essential for Olfactory Memory

STFP-induced LTP in G-M synapses correlates with memory formation after STFP (Figures S1A–S1C), but is it essential for memory formation? To address this question, we ablated Syt10 or the IGF1-R in the MOB of adult *Syt10*$^{f/f}$ or *IGF-1R*$^{f/f}$ mice by

Figure 4. Syt10 Is Essential for STFP-Induced LTP of G-M Synapses

(A) Coronal section of the MOB (left) and cropped region (right) showing layer-specific expression of Syt1 (red) in wild-type (WT) mice.

(B) Example micrographs from the EPL showing localizations of Syt1 puncta (red) relative to vGlut1$^+$ (green) and vGAT$^+$ (blue) synapses.

(C and D) Coronal sections of the MOB (left) and cropped region (right) showing layer-specific expression of Syt10 (green) in WT mice (C) and in Syt10 KO mice (D).

(E and F) Example micrographs from the EPL showing localizations of Syt10 puncta (green) relative to Syt1$^+$ (red) and vGlut1$^+$ (blue) synapses (E) and Syt10 puncta (green) relative to vGlut1$^+$ (red) and vGAT$^+$ (blue) synapses (F). For more data of synaptic localization of Syt1 and Syt10, see Figures S4 and S5.

(G) Example G-M IPSC traces (left), with summarized input-output curves (middle) and curve slopes (right) from M72-associated mitral cells in control (Ctrl) and Syt1 KD MOB slices of naive *M72-GFP* mice. For Syt1 KD efficiency and OS-M EPSC data, see Figures S6A–S6E.

(H) Example G-M IPSC traces (left), with summarized input-output curves (middle) and curve slopes (right) from M72-associated mitral cells in control (Ctrl) and Syt10 KO (Cre) MOB slices of naive *M72-GFP* + *Syt10*$^{f/f}$ mice. For Syt10 KO efficiency, see Figures S6F–S6H.

(I) Schematic diagram showing AAV injection, STFP training, and subsequent slice recordings of G-M IPSCs from M72-associated mitral cells in *M72-GFP* + *Syt10*$^{f/f}$ mice.

(J–L) Example G-M IPSC traces (left), with summarized input-output curves (middle) and curve slopes (right) from M72-associated mitral cells in control (Ctrl) and Syt10 KO (Cre) MOB of *M72-GFP* + *Syt10*$^{f/f}$ observers of plain food (J), Oct food (K), and Acp food (L).

Data in (G), (H), and (J)–(L) are means ± SEM (error bars), with mouse number as sample size n; numbers of neurons/mice are indicated in bars. Statistical analysis is by Student's t test (***$p < 0.001$ and *$p < 0.05$; n.s., $p > 0.1$). Note the images (A, C, and D) were assembled with smaller imaging fields.

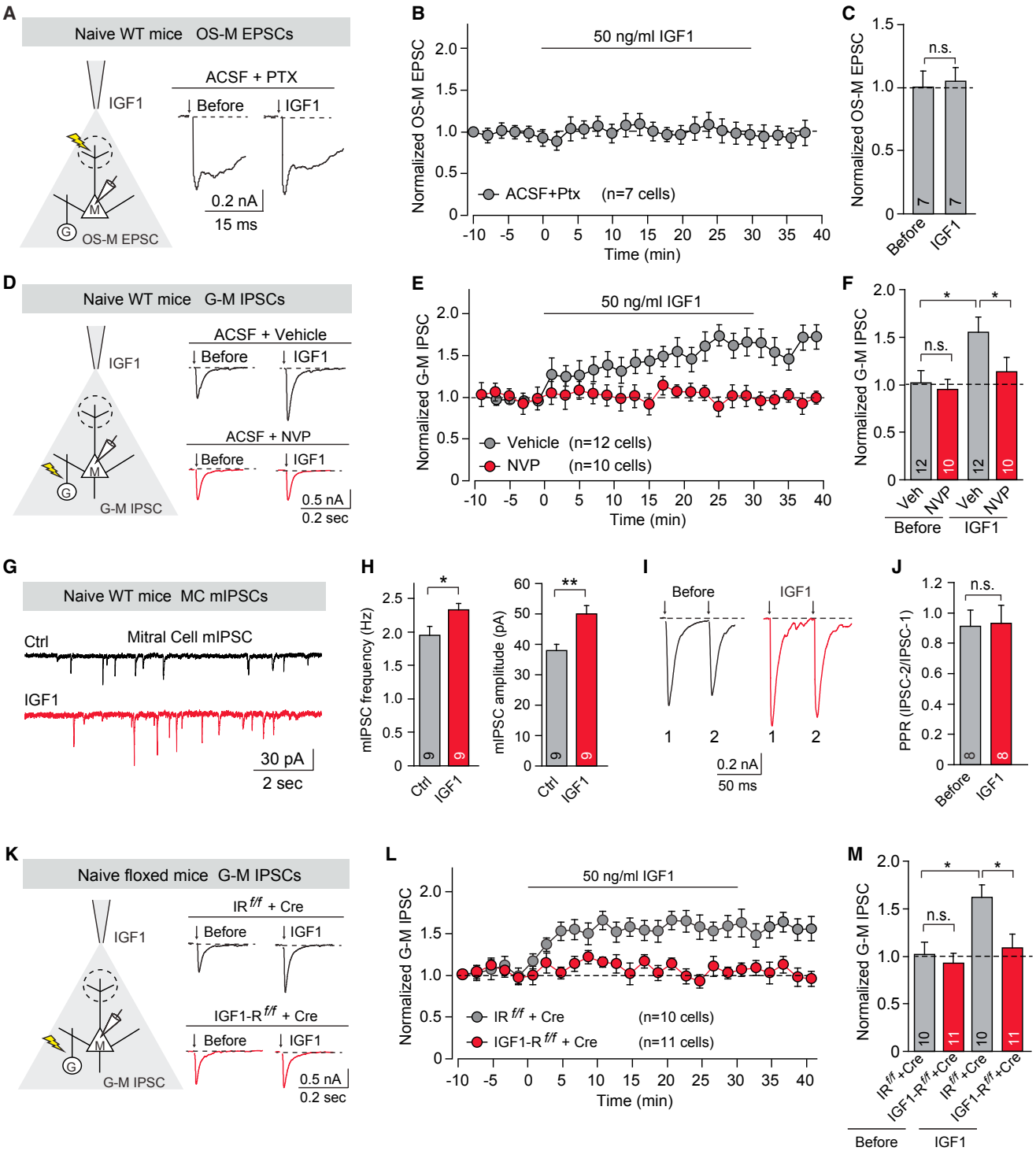

Figure 5. IGF1 Induces Rapid Postsynaptic Potentiation of G-M Synapses Requiring IGF1-R Signaling

(A) IGF1 was applied to acute MOB slices while OS-M EPSCs (example traces, right) were recorded.

(B and C) Summarized time course (B) and normalized amplitude analysis of OS-M EPSCs before and 15–25 min after the initiation of IGF1 application (C), showing no significant effect of IGF1 on the strength of OS-M synaptic transmission.

(D) Acute MOB slices treated with IGF1 with or without pre-incubation of selective IGF1-R kinase inhibitor NVP-AEW541 (1 μM) in ACSF, while G-M IPSCs (example traces, right) were recorded.

(E and F) Summarized time course (E) and normalized amplitude of G-M IPSCs before and 15–25 min after the initiation of IGF1 treatment (F), showing the specificity of IGF1-induced synaptic potentiation.

(legend continued on next page)

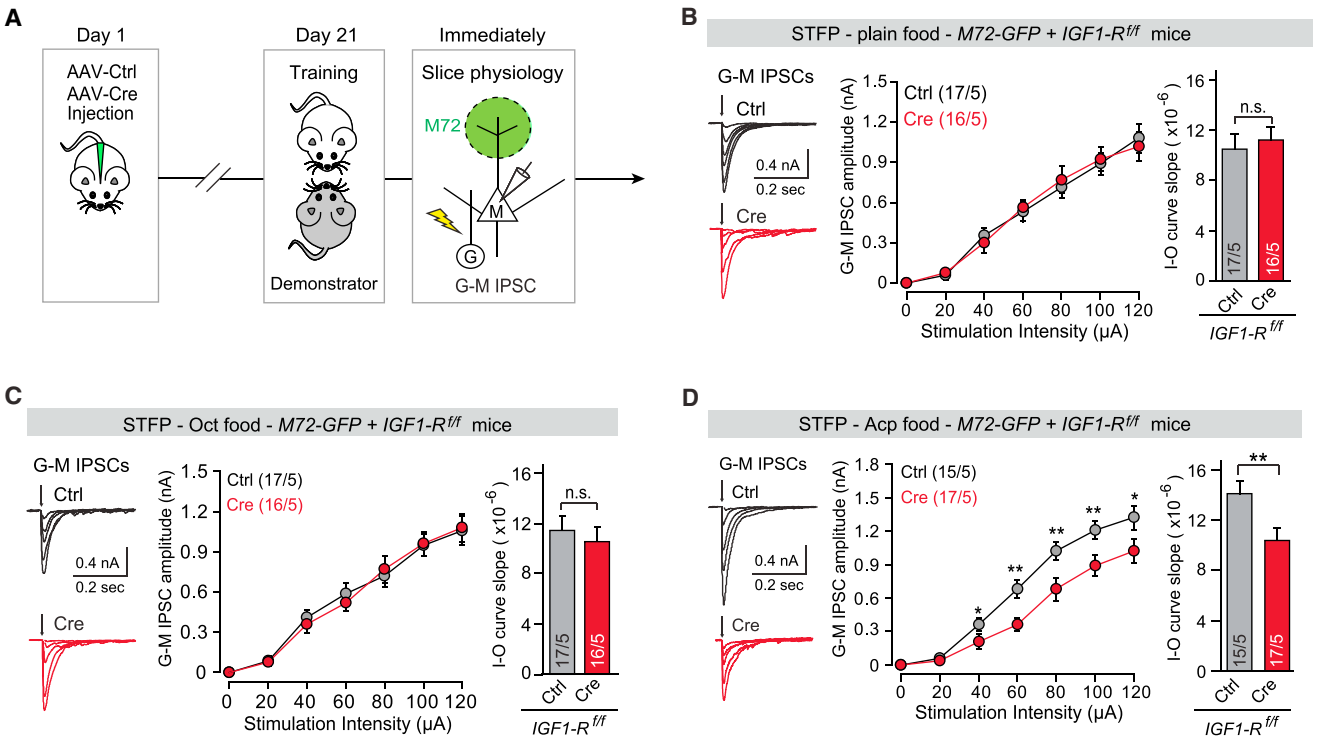

Figure 6. IGF1-R Signaling Is Required by STFP-Induced LTP of G-M Synapses

(A) Schematic diagram showing AAV injection, STFP training, and subsequent slice recordings of G-M IPSCs from M72-associated mitral cells in *M72-GFP* + *IGF1-R$^{f/f}$* mice.

(B–D) Example G-M IPSC traces (left), with summarized input-output curves (middle) and curve slopes (right) from M72-associated mitral cells in control (Ctrl) and IGF1-R KO (Cre) MOBs of *M72-GFP* + *IGF1-R$^{f/f}$* observers of plain food (B), Oct food (C), and Acp food (D). For IGF1-R KO efficiency and basal G-M IPSC data, see Figures S6I and S6J. Data are means ± SEM (error bars), with mouse number as sample size n; numbers of neurons/mice are indicated in bars. Statistical analysis is by Student's t test (**$p < 0.01$ and *$p < 0.05$; n.s., $p > 0.1$).

injecting AAVs encoding Cre-recombinase, which blocks STFP-induced LTP but has no effect on basal synaptic transmission as documented above (Figures 4H, 4L, 6D, and S6J). Complementarily, we ablated Syt1 using AAVs encoding Syt1 shRNAs to impair basal synaptic transmission of G-M synapses as described above (Figure 4G). We subjected the mice with these viral treatments to the behavioral tests of basal olfactory function and memory retrieval after STFP. For all manipulations, appropriate controls were used in parallel as described above, and behavioral analyses were performed in anonymized subjects.

The Syt1 KD severely impaired basal olfactory function, as evidenced by a reduction of olfactory sensitivity (Figures S8A and S8B) and the longer time needed to find a buried food pellet (Figures 7A and 7B). Consequently, the Syt1 KD in the MOB strongly impaired olfactory memory formation after STFP (Figures 7E and 7F), probably because it perturbed olfactory sensory processing. The intrabulbar Syt10 KO, however, had no effect on olfactory sensitivity (Figure S8C) or on food finding (Figure 7C). However, the Syt10 KO significantly impaired olfactory memory formation after STFP, with the impairment increasing in severity over time (Figure 7G). The IGF1-R deletion also had little effect on basal olfactory function (Figures 7D and S8D), but it impaired memory formation similar to the Syt10 KO (Figure 7H). These data indicate that STFP-induced LTP in G-M synapses is essential for olfactory memory formation.

DISCUSSION

Social context modifies all operations of the brain (Behrens et al., 2009), yet the synaptic signature of social context in specific circuits remains unclear. By exploiting reporter mouse lines (*M72-GFP* and *M71-GFP*) in which specific glomeruli with known odorant specificity are labeled by GFP, we here demonstrate that olfactory learning in a social context selectively induces

(G and H) Example mIPSC traces (G), with averaged mIPSC frequency and amplitude (H) of mitral cells with (IGF1) or without (Ctrl) IGF1 treatment.

(I and J) Representative traces (I) and analysis of averaged paired-pulse ratio (PPR) before and during IGF1 treatment (J).

(K) Acute MOB slices with deletions of either IGF1-R or insulin receptor (IR) treated with IGF1, while G-M IPSCs (example traces, right) were recorded.

(L and M) Summarized time courses (L) and normalized amplitude of G-M IPSCs before and 15–25 min after the initiation of IGF1 treatment (M), showing the dominant role of IGF1-R versus IR in IGF1-induced synaptic potentiation. Data are means ± SEM (error bars), with cell number as sample size n; numbers of neurons/mice are indicated in bars. Statistical analysis is by Student's t test (**$p < 0.01$ and *$p < 0.05$; n.s., $p > 0.1$).

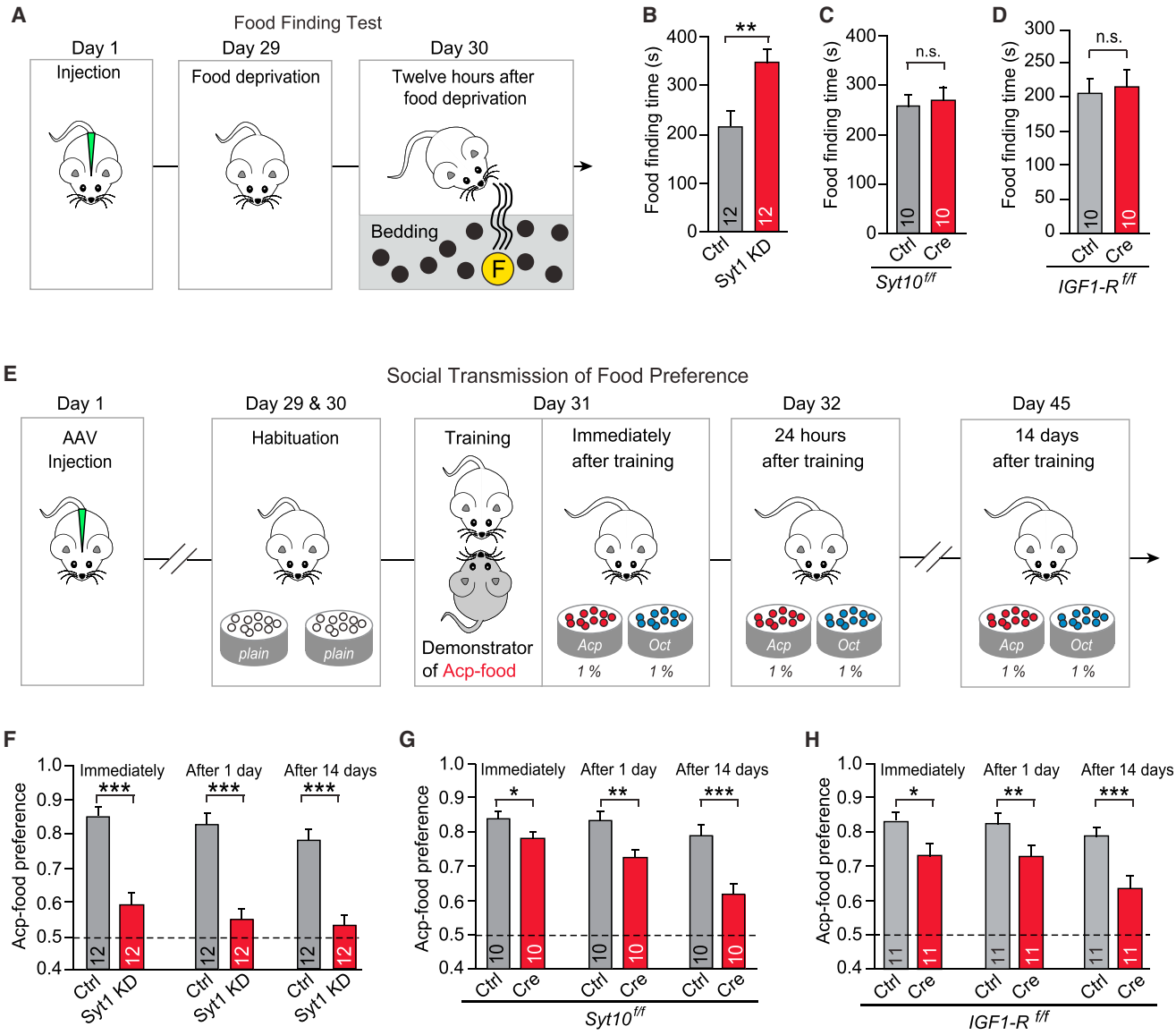

Figure 7. STFP-Induced LTP of G-M Synapses Is Essential for Memory Formation

(A) Schematic diagram showing AAV injection, food deprivation, and subsequent food-finding test.

(B–D) Analyses of time spent in finding buried food by the adult mice with Syt1 KD (B), Syt10 KO (C), and IGF1-R KO (D) in the MOB.

(E) Schematic diagram showing AAV injection, habituation, STFP training, and memory tests after STFP.

(F–H) Analyses of memory retrieval for Acp-flavored food at different time points (immediately, 1 day, and 14 days) after STFP by adult mice with intrabulbar Syt1 KD (F), Syt10 KO (G), and IGF1-R KO (H). For other behavioral tests, see Figure S7.

Data (B–D and F–H) are means ± SEM (error bars), with mouse number as sample size n; numbers of mice are indicated in bars. Statistical analysis is by Student's t test (***$p < 0.001$, **$p < 0.01$, and *$p < 0.05$; n.s., $p > 0.1$).

LTP of the GABAergic component of reciprocal synapses between granule and mitral cells in the MOB (Figures 1 and 2). Strikingly, odor exposure without a social context did not induce this LTP (Figure S3). This socially relevant LTP is preceded by sustained Ca^{2+} transients in the lateral dendrites of mitral cells during social learning (Figure 3). It requires an autocrine and/or paracrine action of IGF1 coupled to IGF1-R signaling to enhance postsynaptic GABA receptor function, as demonstrated by conditional deletion of Syt10, a Ca^{2+} sensor for IGF1 secretion from mitral cell dendrites (Figure 4), and confirmed by IGF1 perfusion (Figure 5) and by conditional deletion of IGF1-R (Figure 6). Finally, we have shown that deletion of Syt10 or the IGF1-R has no effect on olfactory sensation, but it impairs STFP-induced memory formation (Figure 7). Together, these data reveal a socially relevant synaptic modification in a defined microcircuit of the MOB that associates sensory cues with social context during memory encoding (Figure 8). Thus, we propose to have identified a specific event of synaptic plasticity that contributes to memory encoding.

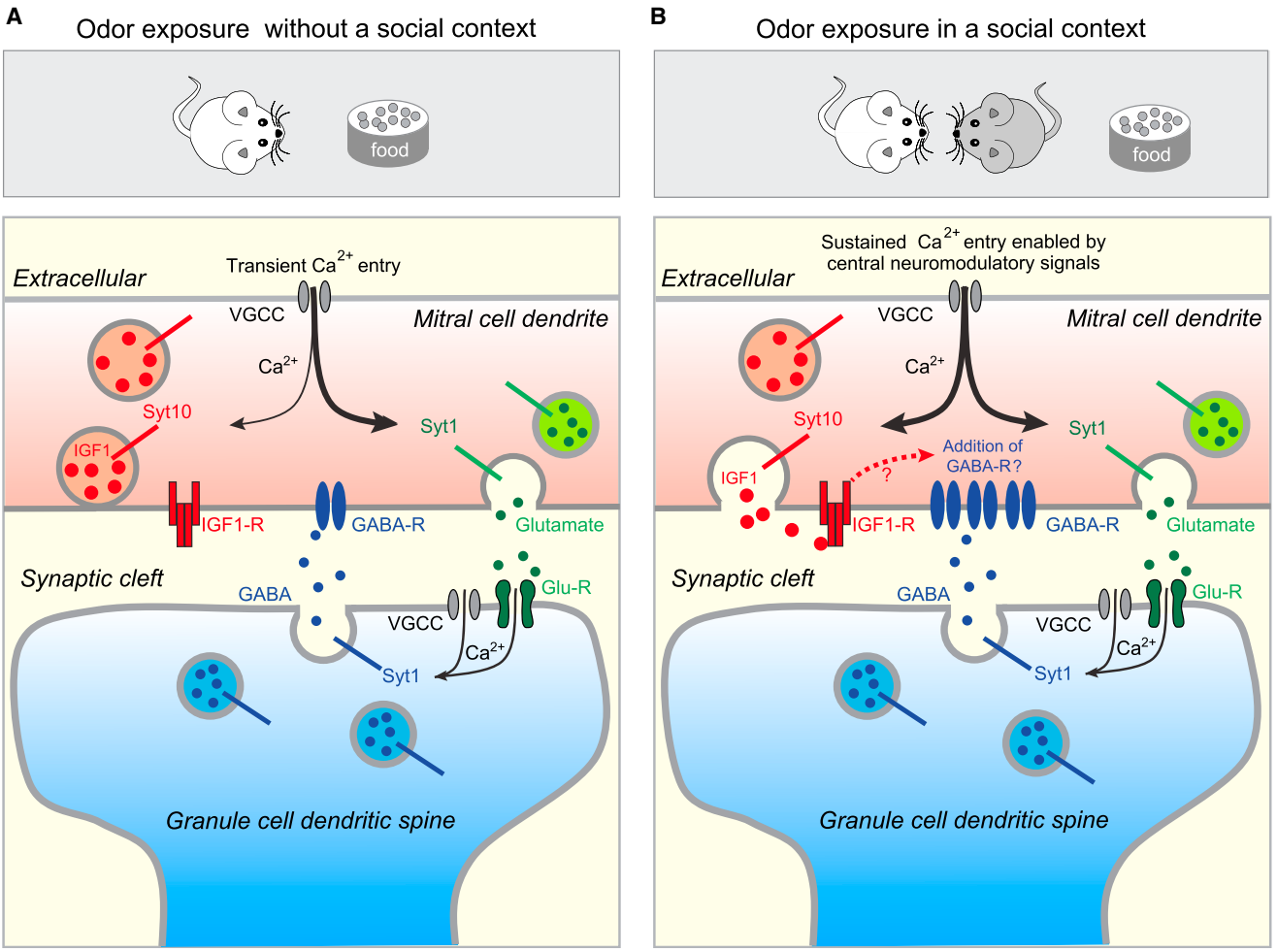

Figure 8. Summarized Diagram Illustrating the Signaling Mechanism of STFP-Induced Potentiation at G-M Synapse

(A) Odor exposure without a social context induces transient Ca^{2+} entry that triggers Syt1-dependent glutamate release, but not Syt10-dependent IGF1 secretion from mitral cell dendrite. Such process then evokes GABA release from granule cell and feedback inhibition on the mitral cell without G-M synaptic potentiation. (B) Odor exposure in a social context during STFP induces sustained Ca^{2+} entry in mitral cell dendrites and triggers both glutamate release and IGF1 exocytosis. IGF1 acts on IGF1-R and potentiates G-M synaptic strength by recruiting more GABA-R, which may be a synaptic substrate for the association of odor signals and social context.

A Synaptic Signature that Associates Social Context with Olfactory Signals

Many brain areas are modulated by diverse types of social behavior (Lin et al., 2005; Gunaydin et al., 2014; Matthews et al., 2016; Li et al., 2016; Okuyama et al., 2016). We asked how social context interacts with sensory processing during social learning. In the MOB, we characterized a long-lasting modification of G-M synapses that is associated with a defined glomerular unit; no synaptic modification was observed in other synapses (OS-M, PG-M, and PV-M), or in G-M synapses that are associated with glomeruli unrelated to the STFP odor. The LTP at G-M synapses was odor specific; STFP with Oct, an odor that is not a ligand of the M72 glomerular unit, did not induce LTP. More importantly, the STFP-induced LTP depended on social context; odor exposure without a social context did not induce LTP. Therefore, this LTP represents a specific synaptic signature that associates social context with food odor signals in the MOB during STFP.

In the MOB, reciprocal M-G-M synapses are critical for sharpening the olfactory tuning profile of mitral cells (Mori et al., 1999; Tan et al., 2010) and for rapid odor discrimination (Abraham et al., 2010; Gschwend et al., 2015). The LTP of GABAergic responses described here would increase the strength of G-M synapses of those glomeruli that were specifically activated during STFP, thus enhancing the ability of mice to selectively discriminate the odor associated with STFP.

STFP-induced LTP, an association mechanism of social context and odor signals, may be recruited by a broader range of social and non-social forms of olfactory learning. Supporting this notion, it has been shown that plasticity of local GABAergic neurons in various species is important for olfactory

adaptive behaviors (Brennan et al., 1990; Keverne and Brennan, 1996; Stopfer and Laurent, 1999; Das et al., 2011).

The hypothesis that memory is encoded by engrams that are formed by modifications of particular synapses is widely favored (Kelleher et al., 2004; Huganir and Nicoll, 2013; Takeuchi et al., 2013). Testing and validating this hypothesis, however, has constituted a persistent challenge because of the difficulty in linking a particular synaptic change to a defined memory. Here, the LTP at G-M synapses induced by social learning from Acp demonstrator mice is essential for the formation of the Acp memory in the observer mice, suggesting that this LTP is part of the engram for odor memory during STFP. However, memory formation is not completely abolished when the STFP-induced M-G-M synapse LTP is ablated by deletions of Syt10 or IGF1-R, suggesting that other synaptic modifications in other brain areas contribute to memory formation after STFP (Lesburguères et al., 2011). Multiple types of synaptic plasticity distributed in different brain regions may coherently contribute to long-term memory formation (Lesburguères et al., 2011; Takeuchi et al., 2013; McGann, 2015).

Signaling Mechanisms Underlying the STFP-Induced LTP

In the present study, we have delineated a signaling pathway whereby odor exposure in the presence of social context induces persistent Ca^{2+} transients in mitral cells (Figure 3), Ca^{2+} then triggers IGF1 secretion via Ca^{2+} binding to Syt10 (Figure 4), and the secreted IGF1 then binds to IGF1-R to potentiate GABAergic G-M sub-synapses (Figures 5 and 6).

Why does odor exposure in the presence of social context induce more persistent Ca^{2+} entry than unconditioned odor exposure? Mice sniffed with similar frequency and amplitude during odor sampling with and without a social context (Figure S3), suggesting that the social context does not change odor-sampling behaviors. Alternatively, activation of centrifugal monoaminergic pathways to the MOB by the social context may be involved (Araneda and Firestein, 2006; Kapoor et al., 2016). For example, serotonin neurons in dorsal raphe nuclei are strongly activated by social interactions (Li et al., 2016), and stimulation of neurons in the raphe nuclei excites mitral cells and strongly promotes their olfactory responses (Kapoor et al., 2016). Moreover, synaptic inputs onto canonical glomerular units from necklace glomeruli that detect semiochemicals may also be involved in the socially relevant sustained Ca^{2+} entry (Munger et al., 2010; Uytingco et al., 2016).

In the present study, the dependence of synaptic plasticity on IGF1 release is not directly addressed by measuring IGF1 release. We did not perform such measurements because IGF1 release in behaving mice is below the detection threshold for neurochemical assays (e.g., ELISA). However, we demonstrated that blocking Ca^{2+}-triggered IGF1 release by the deletion of Syt10 prevents STFP-induced GABAergic LTP (Figure 4) and that blocking IGF1 signaling by the deletion of IGF1-R again prevents STFP-induced LTP (Figure 6). Furthermore, we documented that IGF1 treatment induces LTP at GC-MC synapses (Figure 5). Viewed together, these data link the GABAergic LTP to Ca^{2+}-triggered IGF1 release.

To rule out the possibility that Syt10 performs additional functions in the olfactory bulb besides inducing IGF1 secretion, we performed three lines of control experiments. First, we showed that Syt10 deletion did not alter basal G-M IPSCs in naive mice (Figure 4H). Second, the Syt10 deletion did not impair G-M IPSCs in observer mice that were socially exposed to plain food or Oct food (Figures 4J and 4K), and third, the Syt10 deletion did not impair olfactory sensitivity (Figure S8C), social recognition (Figure S8G), or innate food preference (Figure S8K) in behavioral experiments.

Our study showed that IGF1 selectively potentiates the GABA-R responses of G-M synapses by activating IGF1-Rs, but we have not examined how IGF1-R activation increases GABA-R responses. Stimulation of IGF1-Rs, among others, activates Akt kinases (Fernandez and Torres-Alemán, 2012), and Akt kinases promote trafficking of GABA-Rs (Wang et al., 2003), suggesting that IGF1 may increase GABA-R responses during STFP-induced LTP by an Akt-dependent mechanism. This mechanism may broadly operate throughout the brain (Shcheglovitov et al., 2013; Mardinly et al., 2016).

New Questions

Our results also raise several new questions, some of which have already been alluded to above. First of all, STFP can be considered as a form of associative conditioning, in which food odors and social context may serve as conditioned and unconditioned stimuli, respectively. During STFP training, food odors activate specific glomerular units in the MOB, whereas social context may activate centrifugal neuromodulatory pathways innervating the MOB, or it may directly act on the MOB by stimulating GC-D+ OSNs via carbon disulfide (Munger et al., 2010). Such odor and social signals are then processed by the MOB circuitry via several possible pathways that induce, as a final outcome, the LTP at G-M synapses that we described here. For example, centrifugal neuromodulatory projection from the dorsal raphe nuclei, in which serotonin neurons are specifically activated during social interaction (Li et al., 2016), may provide a social context signal to the MOB. According to this scenario, the olfactory bulb associates odor signals from the MOE with social context signals from serotonin neurons to form LTP at G-M synapses. Alternatively, individual carbon disulfide-sensitive necklace glomeruli that are anatomically and functionally connected to canonical glomeruli (Uytingco et al., 2016) may transfer social carbon disulfide signals to canonical glomeruli for association with odor signals. Exploring these circuits will provide further insight into the mechanisms for olfactory social learning.

Second, we only focused on the STFP-induced LTP within a specific glomerular unit in the present study. It remains to be determined how lateral inhibition (Arevian et al., 2008; Schoppa and Urban, 2003; Wilson and Mainen, 2006) is modulated by the social context. Moreover, given the fact that IGF1 is a diffusible signaling molecule, we do not know how IGF1, as a paracrine factor, alters synaptic function of mitral cells associated with adjacent glomerular units. We have not examined whether the increased GABA-R responses during STFP-induced LTP involve an increase in the GABA-R content of existing synapses, a restructuring of synapses, or even a formation of new synaptic contacts.

Finally, we have not addressed how synaptic turnover resulting from adult neurogenesis (Lepousez et al., 2014) impacts IGF1-dependent LTP and memory encoding during STFP. Answering these questions will be essential for further progress in our understanding of memory formation after social learning. With the identification of social context-dependent LTP, its dependence on IGF1 signaling, and the demonstration of the role of this LTP in olfactory memory in hand, these questions can be addressed now.

STAR★METHODS

Detailed methods are provided in the online version of this paper and include the following:

- KEY RESOURCES TABLE
- CONTACT FOR REAGENT AND RESOURCE SHARING
- EXPERIMENTAL MODEL AND SUBJECT DETAILS
- METHOD DETAILS
  - Virus vector preparation and injection
  - Slice physiology
  - Behavioral tests
  - Fiber photometry analyses
  - Immunohistochemistry and image analyses
  - Immunoblotting
- QUANTIFICATION AND STATISTICAL ANALYSIS

SUPPLEMENTAL INFORMATION

Supplemental Information includes eight figures and can be found with this article online at http://dx.doi.org/10.1016/j.neuron.2017.06.015.

AUTHOR CONTRIBUTIONS

P.C. and T.C.S. designed the experiments and wrote the paper. Z.L., Z.C., C.S., F.Y., Y.S., J.Z., B.Q., H.H., Y.W., and D.L. conducted experiments. Z.L., Z.C., and P.C. analyzed data.

ACKNOWLEDGMENTS

We thank Drs. Minmin Luo and Peter Mombaerts for providing mouse lines. Thanks to Xiaofei Guo and Yan Teng for technical support. This work was supported by the NSFC (81471311, 31422026, and 31671095 to P.C.) and NIH P50 (MH086403 to T.C.S.).

Received: December 23, 2016
Revised: April 17, 2017
Accepted: June 7, 2017
Published: July 5, 2017

REFERENCES

Abraham, N.M., Egger, V., Shimshek, D.R., Renden, R., Fukunaga, I., Sprengel, R., Seeburg, P.H., Klugmann, M., Margrie, T.W., Schaefer, A.T., and Kuner, T. (2010). Synaptic inhibition in the olfactory bulb accelerates odor discrimination in mice. Neuron *65*, 399–411.

Araneda, R.C., and Firestein, S. (2006). Adrenergic enhancement of inhibitory transmission in the accessory olfactory bulb. J. Neurosci. *26*, 3292–3298.

Arevian, A.C., Kapoor, V., and Urban, N.N. (2008). Activity-dependent gating of lateral inhibition in the mouse olfactory bulb. Nat. Neurosci. *11*, 80–87.

Bartlett, W.P., Li, X.S., Williams, M., and Benkovic, S. (1991). Localization of insulin-like growth factor-1 mRNA in murine central nervous system during postnatal development. Dev. Biol. *147*, 239–250.

Behrens, T.E., Hunt, L.T., and Rushworth, M.F. (2009). The computation of social behavior. Science *324*, 1160–1164.

Bourne, J.N., and Schoppa, N.E. (2017). Three-dimensional synaptic analyses of mitral cell and external tufted cell dendrites in rat olfactory bulb glomeruli. J. Comp. Neurol. *525*, 592–609.

Bozza, T., Feinstein, P., Zheng, C., and Mombaerts, P. (2002). Odorant receptor expression defines functional units in the mouse olfactory system. J. Neurosci. *22*, 3033–3043.

Brennan, P., Kaba, H., and Keverne, E.B. (1990). Olfactory recognition: a simple memory system. Science *250*, 1223–1226.

Brüning, J.C., Michael, M.D., Winnay, J.N., Hayashi, T., Hörsch, D., Accili, D., Goodyear, L.J., and Kahn, C.R. (1998). A muscle-specific insulin receptor knockout exhibits features of the metabolic syndrome of NIDDM without altering glucose tolerance. Mol. Cell *2*, 559–569.

Buck, L., and Axel, R. (1991). A novel multigene family may encode odorant receptors: a molecular basis for odor recognition. Cell *65*, 175–187.

Cao, P., Maximov, A., and Südhof, T.C. (2011). Activity-dependent IGF-1 exocytosis is controlled by the Ca(2+)-sensor synaptotagmin-10. Cell *145*, 300–311.

Chen, W.R., Xiong, W., and Shepherd, G.M. (2000). Analysis of relations between NMDA receptors and GABA release at olfactory bulb reciprocal synapses. Neuron *25*, 625–633.

Das, S., Sadanandappa, M.K., Dervan, A., Larkin, A., Lee, J.A., Sudhakaran, I.P., Priya, R., Heidari, R., Holohan, E.E., Pimentel, A., et al. (2011). Plasticity of local GABAergic interneurons drives olfactory habituation. Proc. Natl. Acad. Sci. USA *108*, E646–E654.

De Saint Jan, D., Hirnet, D., Westbrook, G.L., and Charpak, S. (2009). External tufted cells drive the output of olfactory bulb glomeruli. J. Neurosci. *29*, 2043–2052.

Dhawale, A.K., Hagiwara, A., Bhalla, U.S., Murthy, V.N., and Albeanu, D.F. (2010). Non-redundant odor coding by sister mitral cells revealed by light addressable glomeruli in the mouse. Nat. Neurosci. *13*, 1404–1412.

Dietrich, P., Dragatsis, I., Xuan, S., Zeitlin, S., and Efstratiadis, A. (2000). Conditional mutagenesis in mice with heat shock promoter-driven cre transgenes. Mamm. Genome *11*, 196–205.

Fernandez, A.M., and Torres-Alemán, I. (2012). The many faces of insulin-like peptide signalling in the brain. Nat. Rev. Neurosci. *13*, 225–239.

Galef, B.G., Jr. (1982). Studies of social learning in Norway rats: a brief review. Dev. Psychobiol. *15*, 279–295.

Galef, B.G., Jr. (2003). Social learning of food preferences in rodents: rapid appetitive learning. Curr. Protoc. Neurosci. *Chapter 8*, Unit 8.5D.

Galef, B.G., Jr., Mason, J.R., Preti, G., and Bean, N.J. (1988). Carbon disulfide: a semiochemical mediating socially-induced diet choice in rats. Physiol. Behav. *42*, 119–124.

Gariépy, J.F., Watson, K.K., Du, E., Xie, D.L., Erb, J., Amasino, D., and Platt, M.L. (2014). Social learning in humans and other animals. Front. Neurosci. *8*, 58.

Gire, D.H., Franks, K.M., Zak, J.D., Tanaka, K.F., Whitesell, J.D., Mulligan, A.A., Hen, R., and Schoppa, N.E. (2012). Mitral cells in the olfactory bulb are mainly excited through a multistep signaling path. J. Neurosci. *32*, 2964–2975.

Grimm, D., Lee, J.S., Wang, L., Desai, T., Akache, B., Storm, T.A., and Kay, M.A. (2008). In vitro and in vivo gene therapy vector evolution via multispecies interbreeding and retargeting of adeno-associated viruses. J. Virol. *82*, 5887–5911.

Gschwend, O., Abraham, N.M., Lagier, S., Begnaud, F., Rodriguez, I., and Carleton, A. (2015). Neuronal pattern separation in the olfactory bulb improves odor discrimination learning. Nat. Neurosci. *18*, 1474–1482.

Gunaydin, L.A., Grosenick, L., Finkelstein, J.C., Kauvar, I.V., Fenno, L.E., Adhikari, A., Lammel, S., Mirzabekov, J.J., Airan, R.D., Zalocusky, K.A.,

et al. (2014). Natural neural projection dynamics underlying social behavior. Cell *157*, 1535–1551.

Huganir, R.L., and Nicoll, R.A. (2013). AMPARs and synaptic plasticity: the last 25 years. Neuron *80*, 704–717.

Isaacson, J.S., and Strowbridge, B.W. (1998). Olfactory reciprocal synapses: dendritic signaling in the CNS. Neuron *20*, 749–761.

Jahr, C.E., and Nicoll, R.A. (1980). Dendrodendritic inhibition: demonstration with intracellular recording. Science *207*, 1473–1475.

Kapoor, V., Provost, A.C., Agarwal, P., and Murthy, V.N. (2016). Activation of raphe nuclei triggers rapid and distinct effects on parallel olfactory bulb output channels. Nat. Neurosci. *19*, 271–282.

Kato, H.K., Watabe, A.M., and Manabe, T. (2009). Non-Hebbian synaptic plasticity induced by repetitive postsynaptic action potentials. J. Neurosci. *29*, 11153–11160.

Kato, H.K., Gillet, S.N., Peters, A.J., Isaacson, J.S., and Komiyama, T. (2013). Parvalbumin-expressing interneurons linearly control olfactory bulb output. Neuron *80*, 1218–1231.

Kauer, J.S., and Cinelli, A.R. (1993). Are there structural and functional modules in the vertebrate olfactory bulb? Microsc. Res. Tech. *24*, 157–167.

Kelleher, R.J., 3rd, Govindarajan, A., and Tonegawa, S. (2004). Translational regulatory mechanisms in persistent forms of synaptic plasticity. Neuron *44*, 59–73.

Keverne, E.B., and Brennan, P.A. (1996). Olfactory recognition memory. J. Physiol. Paris *90*, 399–401.

Kikuta, S., Fletcher, M.L., Homma, R., Yamasoba, T., and Nagayama, S. (2013). Odorant response properties of individual neurons in an olfactory glomerular module. Neuron *77*, 1122–1135.

Lepousez, G., Nissant, A., Bryant, A.K., Gheusi, G., Greer, C.A., and Lledo, P.M. (2014). Olfactory learning promotes input-specific synaptic plasticity in adult-born neurons. Proc. Natl. Acad. Sci. USA *111*, 13984–13989.

Lesburguères, E., Gobbo, O.L., Alaux-Cantin, S., Hambucken, A., Trifilieff, P., and Bontempi, B. (2011). Early tagging of cortical networks is required for the formation of enduring associative memory. Science *331*, 924–928.

Li, Y., Zhong, W., Wang, D., Feng, Q., Liu, Z., Zhou, J., Jia, C., Hu, F., Zeng, J., Guo, Q., et al. (2016). Serotonin neurons in the dorsal raphe nucleus encode reward signals. Nat. Commun. *7*, 10503.

Lin, D.Y., Zhang, S.Z., Block, E., and Katz, L.C. (2005). Encoding social signals in the mouse main olfactory bulb. Nature *434*, 470–477.

Mardinly, A.R., Spiegel, I., Patrizi, A., Centofante, E., Bazinet, J.E., Tzeng, C.P., Mandel-Brehm, C., Harmin, D.A., Adesnik, H., Fagiolini, M., and Greenberg, M.E. (2016). Sensory experience regulates cortical inhibition by inducing IGF1 in VIP neurons. Nature *531*, 371–375.

Marks, J.L., Porte, D., Jr., and Baskin, D.G. (1991). Localization of type I insulin-like growth factor receptor messenger RNA in the adult rat brain by in situ hybridization. Mol. Endocrinol. *5*, 1158–1168.

Matthews, G.A., Nieh, E.H., Vander Weele, C.M., Halbert, S.A., Pradhan, R.V., Yosafat, A.S., Glober, G.F., Izadmehr, E.M., Thomas, R.E., Lacy, G.D., et al. (2016). Dorsal raphe dopamine neurons represent the experience of social isolation. Cell *164*, 617–631.

McGann, J.P. (2015). Associative learning and sensory neuroplasticity: how does it happen and what is it good for? Learn. Mem. *22*, 567–576.

Migliore, M., Cavarretta, F., Marasco, A., Tulumello, E., Hines, M.L., and Shepherd, G.M. (2015). Synaptic clusters function as odor operators in the olfactory bulb. Proc. Natl. Acad. Sci. USA *112*, 8499–8504.

Miyamichi, K., Shlomai-Fuchs, Y., Shu, M., Weissbourd, B.C., Luo, L., and Mizrahi, A. (2013). Dissecting local circuits: parvalbumin interneurons underlie broad feedback control of olfactory bulb output. Neuron *80*, 1232–1245.

Mombaerts, P., Wang, F., Dulac, C., Chao, S.K., Nemes, A., Mendelsohn, M., Edmondson, J., and Axel, R. (1996). Visualizing an olfactory sensory map. Cell *87*, 675–686.

Mori, K., Nagao, H., and Yoshihara, Y. (1999). The olfactory bulb: coding and processing of odor molecule information. Science *286*, 711–715.

Munger, S.D., Leinders-Zufall, T., McDougall, L.M., Cockerham, R.E., Schmid, A., Wandernoth, P., Wennemuth, G., Biel, M., Zufall, F., and Kelliher, K.R. (2010). An olfactory subsystem that detects carbon disulfide and mediates food-related social learning. Curr. Biol. *20*, 1438–1444.

Najac, M., De Saint Jan, D., Reguero, L., Grandes, P., and Charpak, S. (2011). Monosynaptic and polysynaptic feed-forward inputs to mitral cells from olfactory sensory neurons. J. Neurosci. *31*, 8722–8729.

Okuyama, T., Kitamura, T., Roy, D.S., Itohara, S., and Tonegawa, S. (2016). Ventral CA1 neurons store social memory. Science *353*, 1536–1541.

Potter, S.M., Zheng, C., Koos, D.S., Feinstein, P., Fraser, S.E., and Mombaerts, P. (2001). Structure and emergence of specific olfactory glomeruli in the mouse. J. Neurosci. *21*, 9713–9723.

Ressler, K.J., Sullivan, S.L., and Buck, L.B. (1994). Information coding in the olfactory system: evidence for a stereotyped and highly organized epitope map in the olfactory bulb. Cell *79*, 1245–1255.

Schoppa, N.E., and Urban, N.N. (2003). Dendritic processing within olfactory bulb circuits. Trends Neurosci. *26*, 501–506.

Schoppa, N.E., Kinzie, J.M., Sahara, Y., Segerson, T.P., and Westbrook, G.L. (1998). Dendrodendritic inhibition in the olfactory bulb is driven by NMDA receptors. J. Neurosci. *18*, 6790–6802.

Scolnick, J.A., Cui, K., Duggan, C.D., Xuan, S., Yuan, X.B., Efstratiadis, A., and Ngai, J. (2008). Role of IGF signaling in olfactory sensory map formation and axon guidance. Neuron *57*, 847–857.

Serizawa, S., Miyamichi, K., Nakatani, H., Suzuki, M., Saito, M., Yoshihara, Y., and Sakano, H. (2003). Negative feedback regulation ensures the one receptor-one olfactory neuron rule in mouse. Science *302*, 2088–2094.

Shao, Z., Puche, A.C., Liu, S., and Shipley, M.T. (2012). Intraglomerular inhibition shapes the strength and temporal structure of glomerular output. J. Neurophysiol. *108*, 782–793.

Shcheglovitov, A., Shcheglovitova, O., Yazawa, M., Portmann, T., Shu, R., Sebastiano, V., Krawisz, A., Froehlich, W., Bernstein, J.A., Hallmayer, J.F., and Dolmetsch, R.E. (2013). SHANK3 and IGF1 restore synaptic deficits in neurons from 22q13 deletion syndrome patients. Nature *503*, 267–271.

Shepherd, G.M., Chen, W.R., and Greer, C.A. (2004). Olfactory bulb. In The Synaptic Organization of the Brain, G.M. Shepherd, ed. (Oxford University Press), pp. 165–217.

Shepherd, G.M., Chen, W.R., Willhite, D., Migliore, M., and Greer, C.A. (2007). The olfactory granule cell: from classical enigma to central role in olfactory processing. Brain Res. Brain Res. Rev. *55*, 373–382.

Stewart, W.B., Kauer, J.S., and Shepherd, G.M. (1979). Functional organization of rat olfactory bulb analysed by the 2-deoxyglucose method. J. Comp. Neurol. *185*, 715–734.

Stopfer, M., and Laurent, G. (1999). Short-term memory in olfactory network dynamics. Nature *402*, 664–668.

Südhof, T.C. (2013). A molecular machine for neurotransmitter release: synaptotagmin and beyond. Nat. Med. *19*, 1227–1231.

Takeuchi, T., Duszkiewicz, A.J., and Morris, R.G. (2013). The synaptic plasticity and memory hypothesis: encoding, storage and persistence. Philos. Trans. R. Soc. Lond. B Biol. Sci. *369*, 20130288.

Tan, J., Savigner, A., Ma, M., and Luo, M. (2010). Odor information processing by the olfactory bulb analyzed in gene-targeted mice. Neuron *65*, 912–926.

Tobin, V.A., Hashimoto, H., Wacker, D.W., Takayanagi, Y., Langnaese, K., Caquineau, C., Noack, J., Landgraf, R., Onaka, T., Leng, G., et al. (2010). An intrinsic vasopressin system in the olfactory bulb is involved in social recognition. Nature *464*, 413–417.

Uchida, N., Poo, C., and Haddad, R. (2014). Coding and transformations in the olfactory system. Annu. Rev. Neurosci. *37*, 363–385.

Uytingco, C.R., Puche, A.C., and Munger, S.D. (2016). Interglomerular connectivity within the canonical and GC-D/necklace olfactory subsystems. PLoS ONE *11*, e0165343.

Vaaga, C.E., and Westbrook, G.L. (2016). Parallel processing of afferent olfactory sensory information. J. Physiol. *594*, 6715–6732.

Vincis, R., Gschwend, O., Bhaukaurally, K., Beroud, J., and Carleton, A. (2012). Dense representation of natural odorants in the mouse olfactory bulb. Nat. Neurosci. *15*, 537–539.

Wachowiak, M., Economo, M.N., Díaz-Quesada, M., Brunert, D., Wesson, D.W., White, J.A., and Rothermel, M. (2013). Optical dissection of odor information processing in vivo using GCaMPs expressed in specified cell types of the olfactory bulb. J. Neurosci. *33*, 5285–5300.

Wang, Q., Liu, L., Pei, L., Ju, W., Ahmadian, G., Lu, J., Wang, Y., Liu, F., and Wang, Y.T. (2003). Control of synaptic strength, a novel function of Akt. Neuron *38*, 915–928.

Wesson, D.W., Donahou, T.N., Johnson, M.O., and Wachowiak, M. (2008). Sniffing behavior of mice during performance in odor-guided tasks. Chem. Senses *33*, 581–596.

Willhite, D.C., Nguyen, K.T., Masurkar, A.V., Greer, C.A., Shepherd, G.M., and Chen, W.R. (2006). Viral tracing identifies distributed columnar organization in the olfactory bulb. Proc. Natl. Acad. Sci. USA *103*, 12592–12597.

Wilson, R.I., and Mainen, Z.F. (2006). Early events in olfactory processing. Annu. Rev. Neurosci. *29*, 163–201.

Witt, R.M., Galligan, M.M., Despinoy, J.R., and Segal, R. (2009). Olfactory behavioral testing in the adult mouse. J. Vis. Exp. (23), 949.

Wrenn, C.C. (2004). Social transmission of food preference in mice. Curr. Protoc. Neurosci. *Chapter 8*, Unit 8.5G.

Xu, W., Morishita, W., Buckmaster, P.S., Pang, Z.P., Malenka, R.C., and Südhof, T.C. (2012). Distinct neuronal coding schemes in memory revealed by selective erasure of fast synchronous synaptic transmission. Neuron *73*, 990–1001.

Zhang, J., Huang, G., Dewan, A., Feinstein, P., and Bozza, T. (2012). Uncoupling stimulus specificity and glomerular position in the mouse olfactory system. Mol. Cell. Neurosci. *51*, 79–88.

STAR★METHODS

KEY RESOURCES TABLE

REAGENT or RESOURCE	SOURCE	IDENTIFIER
Antibodies		
GFP	Abcam	Cat. No. ab290; RRID: AB_303395
Syt1	Synaptic System	Cat. No. 105002; RRID: AB_887830
Syt10	NeuroMab	Cat. No. 75-262; RRID: AB_10671950
vGlut1	Millipore	Cat. No. AB5905; RRID: AB_2301751
vGAT	Millipore	Cat. No. AB5062P; RRID: AB_2301998
parvalbumin	Millipore	Cat. No. MAB1572; RRID: AB_11211313
IGF1-R	Abcam	Cat. No. ab131476; RRID: AB_11155487
GAPDH	Cell Signaling	Cat. No. 5174; RRID: AB_10622025
Bacterial and Virus Strains		
AAV-Syt1 KD	Stanford Vector Core	N/A
AAV-GFP	Stanford Vector Core	N/A
AAV-Cre	Stanford Vector Core	N/A
AAV-DIO-GCaMP6m	Stanford Vector Core	N/A
Chemicals, Peptides, and Recombinant Proteins		
D-AP5 / CNQX	Tocris	Cat. No. 0106 / Cat. No. 0190
Picrotoxin	Tocris	Cat. No. 1128
TTX	Tocris	Cat. No. 1078
IGF1	R&D Systems	Cat. No. 791-MG
NVP-AEW541	Selleckchem	Cat. No. S1034
Experimental Models: Organisms/Strains		
M72-GFP	JAX Mice	Stock No: 007766
M71-GFP	JAX Mice	Stock No: 006676
Syt10 f/f	JAX Mice	Stock No: 008413
IGF1-R f/f	JAX Mice	Stock No: 012251
IR f/f	JAX Mice	Stock No: 006955
Ai9	JAX Mice	Stock No: 007905
PV-ires-Cre	JAX Mice	Stock No: 008069
Cdhr1-Cre	MMRRC	STOCK Tg(Cdhr1-cre)KG66Gsat/Mmucd
Software and Algorithms		
Clampfit 10.4	Molecular Devices	https://www.moleculardevices.com
ImageJ	NIH	https://imagej.nih.gov/ij/
Other		
Fiber photometry system	ThinkerTech, Nanjing	FIS
Patch clamp system	Molecular Devices	MultiClamp 700B
Confocal imaging system	Olympus	FV1200

CONTACT FOR REAGENT AND RESOURCE SHARING

Further information and requests for resources and reagents should be directed to and will be fulfilled by the Lead Contact, Peng Cao (caopeng@nibs.ac.cn).

EXPERIMENTAL MODEL AND SUBJECT DETAILS

All experimental procedures were conducted following protocols approved by the Administrative Panel on Laboratory Animal Care at the Institute of Biophysics, Chinese Academy of Sciences. Mice were maintained in specific-pathogen-free mouse facility on a circadian cycle of 12-h light and 12-h dark, with food and water available ad libitum. Adult mice were housed in groups (3 to 5 animals per cage) before they were separated one week prior to experiments. The generation of *Syt10*$^{f/f}$ mice was described previously (Cao et al., 2011). *IGF1-R* $^{f/f}$ and *IR* $^{f/f}$ mice were imported from Jackson Laboratory. *M72-GFP* and *M71-GFP* mice, which are available in JAX Mice, were imported from Dr. Minmin Luo's Laboratory at the National Institute of Biological Sciences with approval from Dr. Peter Mombaerts at the Max Planck Institute of Biophysics. No statistical tests were used to predetermine sample size.

Adult mice (age between 3 to 5 months old) with or without prior viral injections were used for slice physiology or behavioral tests. For STFP experiments and subsequent slice physiology, the observer mice were either male or female, whereas demonstrator mice were always female. For other behavioral experiments, mice were either male or female. To knockdown Syt1, AAV-Syt1 KD or AAV-GFP was stereotaxically injected into the bilateral olfactory bulbs of *M72-GFP* mice. To delete Syt10, IGF1-R or IR, AAV-Cre or AAV-GFP was injected into the bilateral olfactory bulbs of *M72-GFP/Syt10*$^{f/f}$, *M72-GFP/IGF1*$^{f/f}$ or *M72-GFP/IR* $^{f/f}$ mice. To specifically label mitral cells with GCaMP6, AAV-DIO-GCaMP6 was injected into the ipsilateral olfactory bulb of *Cdhr1-Cre* mice, followed by optic fiber implantation into the EPL.

METHOD DETAILS

Virus vector preparation and injection

The serotype for adeno-associated virus (AAV) in this study was AAV-DJ (Grimm et al., 2008), which was packaged by Dr. Lochrie's team at the Stanford Gene Vector and Virus Core. The final viral vector titers were in the range of 1-5 × 10^{12} particles/ml. Two-month old mice were anesthetized with tribromoethanol (125-250 mg/kg). Viral vectors were bilaterally injected with a glass pipette at a flow rate of 0.15 μl/min. The coordinates used for MOB injection were bregma 4.75 mm, lateral ± 1.1 mm and dura −1.25 mm.

Slice physiology

MOB slice preparation

Acute MOB slices were prepared from adult mice anesthetized with isofluorane before decapitation. Brains were rapidly removed and placed in ice-cold oxygenated (95% O_2 and 5% CO_2) cutting solution (228 mM sucrose, 11 mM glucose, 26 mM $NaHCO_3$, 1 mM NaH_2PO_4, 2.5 mM KCl, 7 mM $MgSO_4$ and 0.5 mM $CaCl_2$). Coronal MOB slices (300 μm) were cut using a vibratome (VT 1200S, Leica Microsystems, Wetzlar, Germany). The slices were incubated at 28°C in oxygenated artificial cerebrospinal fluid (ACSF: 119 mM NaCl, 2.5 mM KCl, 1 mM NaH_2PO_4, 1.3 mM $MgSO_4$, 26 mM $NaHCO_3$, 10 mM glucose, and 2.5 mM $CaCl_2$) for 30 min, and were then kept at room temperature under the same conditions for 1 hr before transfer to the recording chamber at 25°C. The ACSF was perfused at 1 mL / min.

Whole-cell recording

The MOB slices were visualized with a 40 × water immersion lens, differential interference contrast (DIC) optics and a CCD camera (Q-Imaging Rolera-XR, BC, Canada). Patch pipettes were pulled from borosilicate glass pipettes (diameter 1.5 mm) using a PC-10 pipette puller. For voltage clamp recordings of the postsynaptic currents, pipettes were filled with internal solution (in mM, 135 CsCl, 10 HEPES, 1 EGTA, 1 Na-GTP and 4 Mg-ATP and 2% neurobiotin, pH 7.25). For recording membrane depolarization-induced G-M IPSCs from mitral cells (recurrent inhibition), pipettes were filled with internal solution (in mM, 120 CsCl,10 TEA-Cl,20 HEPES,3 ATP-Mg,0.2 Na-GTP,0.2 EGTA). The membrane potentials of mitral cells and granule cells were always held at −70 mV. The resistance of pipettes varied between 3.0–3.5 MΩ. The whole-cell current signals were recorded with MultiClamp 700B and Clampex 10 data acquisition software. After establishment of the whole-cell configuration and equilibration of the intracellular pipette solution with the cytoplasm, series resistance was compensated to 10–15 MΩ. Recordings with series resistances that exceeded 15 MΩ were rejected.

Identification and verification of M72/M71-associated mitral cells in MOB slices

The GFP^+ M72/M71 glomeruli in acute olfactory slices were visualized under the microscope for slice physiology, and imaged with the CCD camera and Image-Pro Plus. Two criteria were simultaneously used to identify mitral cells putatively associated with the M72/M71 glomeruli: First, in the presence of picrotoxin, putative M72/M71 mitral cells responded to electrical stimulation in the GFP^+ glomerulus with an evoked excitatory postsynaptic current blocked by D-AP5 and CNQX (Figure S1G). Second, the primary dendrites of mitral cells were visibly extending to M72 glomerulus under the microscope.

Recording of OS-M EPSCs or PG-M IPSCs from M72-associated mitral cells

M72-associated mitral cells were recorded while a bipolar stimulation electrode (FHC, CBAEC75 Concentric Bipolar Electrode OP: 125 μm SS; IP: 25 μm Pt/Ir) was positioned within the GFP^+ glomerulus with stimulus pulses (1 ms, 0.067 Hz, 20∼120 μA) generated by an AMPI isolator triggered by Clampex Software. ACSF with $GABA_A$ receptor antagonist (picrotoxin, PTX, 50 μM) or glutamate receptor antagonists (D-AP5 50 μM and CNQX 20 μM) were respectively perfused to the MOB slice to pharmacologically isolate OS-M EPSCs or PG-M IPSCs. To assure the stimulus was similar across different slices, the tip of stimulation electrode was carefully adjusted to ∼20 μm below the surface of each slice. For validation of OS-M EPSC and PG-M IPSC, see Figure S1.

Recording of PV-M IPSCs from M72-associated mitral cells

M72-associated mitral cells were recorded while light stimulations (laser 473 nm, single pulse, 0.067 Hz, duration 5 ms, 20 mW) were applied to ChR2-expressing PV^+ neurons in the acute MOB slices from *M72-GFP* + *PV-ires-Cre* + *Ai32* mice (Figures S2C–S2E). D-AP5 (50 μM) and CNQX (20 μM) were perfused in ACSF.

Recording of M-G-M IPSCs from M72-associated mitral cells

Recurrent inhibition of mitral cells was measured by depolarizing membrane potential of mitral cells for 10 ms from −70 mV to 0 mV, with TTX in ACSF and TEA-Cl in the pipette internal solution. For validation of M-G-M IPSC, see Figures S2A and S2B.

Recording of M-G EPSCs from granule cells associated with M72 mitral cells

Granule cells associated with M72 mitral cells were recorded while local stimulation was delivered by a bipolar electrode in the granule cell layer, with a distance of ~50 μm away from the mitral cell body (Figure S2I). To assure the stimulus was similar across different slices, the tip of stimulation electrode was carefully adjusted to ~20 μm below the surface of each slice. For validation of M-G EPSCs, PTX (50 μM) was perfused in ACSF (Figure S2J).

Recording of G-M IPSCs from M72-associated mitral cells

M72-associated mitral cells were recorded while a bipolar stimulation electrode was positioned in granule cell layer, with a distance of ~50 μm away from the mitral cell body (Figures S2F and S2G). To assure the stimulus was similar across different slices, the tip of stimulation electrode was carefully adjusted to ~20 μm below the surface of each slice. D-AP5 (50 μM) and CNQX (20 μM) were perfused in ACSF. For validation of G-M IPSC, see Figure S2H.

Recording of mIPSCs of M72-associated mitral cells or mEPSCs of granule cells associated with M72 mitral cells

mIPSCs of M72-associated mitral cells were recorded with TTX (1 μM), D-AP5 (50 μM) and CNQX (20 μM) in ACSF. mEPSCs of granule cells associated with M72 mitral cells were recorded with TTX (1 μM) and PTX (50 μM) in ACSF.

Recording GABA-induced IPSCs from M72-associated mitral cells

A pipette containing ACSF with 100 μM GABA was positioned above the dendrite of M72-associated mitral cells. Controlled by Picospritzer III, GABA puff was delivered at 5 psi for 1 s while M72-associated mitral cells were recorded at voltage clamp mode at −70 mV in the presence of D-AP5 (50 μM) and CNQX (20 μM) in ACSF.

Testing IGF1 effect on G-M IPSCs

In the experiments to test IGF1 effect on G-M IPSCs, IGF1 (50 ng/ml) and selective IGF1-R inhibitor NVP-AEW541 (1 μM, Selleckchem) were delivered to the acute MOB slices via a computer-controlled multi-channel drug delivery system (Yi-Bo Life Science Instruments). The series resistance of the recorded mitral cell was always monitored. Recordings with series resistance exceeding 18 MΩ were rejected.

Behavioral tests

General

All behavioral tests were conducted with male mice during the same circadian period (13:00–18:00). The mice were housed individually one week before the behavioral tests and were handled daily by the experimenters for at least three days before the behavioral tests. The mice were transferred to the testing room and were habituated to the room conditions for 3 hr before the experiments started. The apparatus was cleaned with 20% ethanol to eliminate odor cues from other mice. All behaviors were scored by experimenters who were blind to the treatment of the animals. All odor chemicals (acetophenone, octanal and isoamyl acetate) were from Sigma-Aldrich.

Food-finding test

The food-finding test was performed as described previously (Cao et al., 2011). Following 18 hr food deprivation, the mice were moved to a new cage where a single food pellet was buried randomly in one corner. The latency for food finding was measured before the mice were returned to their home cages.

Olfactory sensitivity test

In the olfactory sensitivity test, mice were exposed to filter paper containing isoamyl acetate (IAA) of different concentrations (zero, 0.001%, 0.01%, 0.1% and 1%). Time spent sniffing the filter paper was measured to quantify olfactory sensitivity (Witt et al., 2009).

Social discrimination test

In the social discrimination test, a young 3-week-old mouse was placed into the home cage of a test adult mouse. Time spent by the test mouse investigating the young mouse was measured. Ten minutes later, the familiar young mouse and an unfamiliar young mouse were both placed in the home cage of the test mouse. Time spent by the test mouse investigating the familiar and unfamiliar young mice was measured again, and total investigation time and social discrimination ratio (time spent investigating unfamiliar mice relative to total investigation time) were calculated (Tobin et al., 2010).

Innate food preference test

Food pellet with Acp (1%) and Oct (1%) were baked in an oven (55°C, 2 hours) until the food cookies are completely dry. Although the initial concentration of Acp or Oct during food mixing was 1%, the final concentration after baking is much lower than this value. In the innate food preference test, two days before the innate food preference test, food-deprived (18 h) mice naive to tested odors were placed into a cage with two bottles containing plain food, where they were habituated to eating food pellet from bottles. On the day of STFP training, the mice were moved to the same cage with two bottles containing food flavored with Acp and Oct. The positioning of the food bottles was randomly selected to avoid position preference of the observer mice. The mice were allowed to eat the different

food for 60 min before being returned to their home cages. The consumed Acp-flavored or Oct-flavored food was measured and their ratios to total food consumption were calculated.

Social transmission of food preference (STFP) test

STFP test was performed according to standard protocol (Figure S1). Two days before training, food-deprived (12 h) observer mice naive to tested odors were placed into a cage with two bottles containing plain food, where they were habituated to eating food pellet from bottles. In a similar way, the food-deprived demonstrator mice were habituated to eating food pellet with Acp (1%) from bottles. On the day of training, the demonstrator mice were allowed to eat Acp-flavored food for 30 min, and were then put into the home cage of the observer mice for social interaction (30 min). Immediately, 1 day or 14 days after social interaction, the observer mice were placed into the cage with two bottles containing Acp-flavored and Oct-flavored food. The positioning of the Acp-flavored and Oct-flavored food bottles was random to avoid position preference of the observer mice. They were allowed to eat the different food for 60 min before being returned to their home cages. The consumed Acp-flavored or Oct-flavored food was measured and their ratios to total food consumption were calculated. To avoid fighting between observer and demonstrator, the demonstrator mice were always female. STFP was also combined with slice physiology (Figure 1A). *M72-GFP* mice were subjected to STFP training with wild-type demonstrators that had ingested plain food, Oct-flavored or Acp-flavored food. Immediately, 1 day or 14 days after STFP training, they were subjected to slice physiology to identify the synaptic modifications in the MOB by STFP.

Sniffing behavior measurement

Sniffing behavior was performed according to standard protocol (Wesson et al., 2008). One week before sniffing recording, mice were implanted with an intranasal cannula during anesthesia. On the day of recording, the intranasal cannula was connected to the pressure transducer by a piece of polyethylene tubing. During experiment, sniffing of freely moving mice was monitored by measuring intranasal respiratory pressure. The voltage was amplified 100X, low-pass filtered at 100 Hz, and digitized at 8000 Hz with Spike 2 Software.

Fiber photometry analyses

Fiber photometry recording was performed with a commercialized fiber photometry system (Model FIS, ThinkerTech). AAV-DIO-GCaMP6m was stereotaxically injected into the mitral cell layer of the MOB of Cdhr1-Cre mice, followed by implantation of optic fiber (230 μm O.D., 0.37 numerical aperture; Shanghai Fiblaser) at external plexiform layer. The coordinates for injection (bregma 4.50 mm, lateral ± 1.30 mm and dura −0.5 mm) and implantation was carefully adjusted so that the tip of optic fiber was close to the rostral M72 glomerular unit (bregma 4.50 mm, lateral ± 1.30 mm and dura −0.1 mm). Fiber recordings were performed in freely moving mice three weeks after virus injection. To induce fluorescence signals (Figure 3D), a laser beam from a laser tube (488 nm) was reflected by a dichroic mirror, focused by a 10x len (NA = 0.3) and then coupled to an optical commutator. A 2-m optical fiber (230 μm O.D., NA = 0.37) guided the light between the commutator and the implanted optical fiber. To minimize photo bleaching, the power intensity at the fiber tip was adjusted to 0.02 mW. The GCaMP6m fluorescence was band-pass filtered (MF525-39, Thorlabs) and collected by a photomultiplier tube (R3896, Hamamatsu). An amplifier (C7319, Hamamatsu) was used to convert the photomultiplier tube current output to voltage signals, which was further filtered through a low-pass filter (40 Hz cut-off; Brownlee 440). The analog voltage signals were digitalized at 100 Hz and recorded by a Power 1401 digitizer and Spike2 software (CED, Cambridge, UK). Recorded fluorescence from each continuous experimental trial was normalized to the averaged fluorescence one second before the initiation of the trial.

Immunohistochemistry and image analyses

Mice were anesthetized with isoflurane and sequentially perfused with saline and phosphate buffered saline (PBS) containing 4% paraformaldehyde (PFA). Brains were removed, post-fixed overnight, and incubated in PBS containing 30% sucrose until they sunk to the bottom. Cryostat coronal sections (40 μm) containing the MOB, the piriform cortex or the entorhinal cortex were collected, incubated overnight with blocking solution (PBS containing 10% goat serum and 0.7% Triton X-100), and then treated with primary antibodies diluted with blocking solution for 8∼12 hr at room temperature. Primary antibodies were washed three times with washing buffer (PBS containing 0.7% Triton X-100) before incubation with secondary antibodies (tagged with Cy2, Cy3 or Cy5, 1:500) for 1 hr at room temperature. Sections were again washed three times with washing buffer, transferred onto Super Frost slides, and mounted under glass coverslips with mounting media. Primary antibodies used for immunohistochemistry included GFP (Abcam ab290, 1:2000), Syt1 (Synaptic System, 105002, 1:1000), Syt10 (NeuroMab, 75-262, 1:500), vGlut1 (Millipore AB5905, 1:1000), vGAT (Millipore AB5062P, 1:500) and parvalbumin (Millipore MAB1572, 1:500). Sections were imaged with a Nikon epifluorescence microscope (4 × and 10 × objectives) or an Olympus FV1200 confocal microscope (60 × and 100 × oil-immersion objective). Samples were excited by 488, 543 or 633 nm lasers in sequential acquisition mode to avoid signal leaking. Identical acquisition settings were applied to all samples in the same batch of experiments. Saturation was avoided by monitoring pixel intensity with Hi-Lo mode. Puncta diameter was analyzed with ImageJ. In brief, the scale of the pictures was set in NIH ImageJ based on the physical dimension of the picture recorded by the confocal system. After converting the pictures from red–green–blue color mode to 16-bit mode, the puncta in the pictures were binarized and measured automatically by NIH ImageJ. To plot the cumulative distribution curves, 300–400 puncta for each label were used. Each pair of distribution curves was tested statistically with the Kolmogorov-Smirnov test. Colocalization analyses were done using NIH ImageJ plug-in JACoP. Although the JACoP plug-in can automatically calculate the Pearson's

coefficient (PC), the raw PC needs to be corrected by subtracting the background PC, which was obtained by translating one of the images for 15 pixels in both directions.

Immunoblotting

Immunoblotting was used to verify the efficiency of deletion or knockdown of individual genes in the adult MOB. Equivalent amounts of protein samples were loaded and resolved in SDS-PAGE (10%) and subsequently transferred to polyvinylidene difluoride (PVDF) membranes. The PVDF membranes were blocked in Tris-buffered saline containing Tween 20 (TBST) with 5% non-fat dry milk for 1 hr. The membrane was then incubated with the primary antibody overnight at 4°C, then incubated with horseradish peroxidase-linked goat anti-rabbit or anti-mouse IgG (1:10000) and developed using peroxidase chemiluminescent reaction (ECL). Primary antibodies used in immunoblotting included Syt1 (Synaptic System, 105002, 1:1000), Syt10 (NeuroMab 75-262, 1:1000), IGF1-R (Abcam ab131476, 1:500) and GAPDH (Cell Signaling 5174, 1:1000).

QUANTIFICATION AND STATISTICAL ANALYSIS

All experiments of slice physiology, behavioral tests and morphological analyses were performed with anonymized sample in which the experimenter was unaware of the experimental condition of mice. Student's t test was used to analyze slice physiology data (Figures 1, 2, 4, 5, 6, S1–S3, S6, and S7), fiber photometry data (Figure 3) and behavioral data (Figures 7, S1, S3, and S8). The Kolmogorov-Smirnov test was used to analyze the cumulative curves of mEPSCs / mIPSCs (Figure 2) or puncta diameter (Figure S5). The "*n*" used for these analyses represents number of mice (Figures 1, 2, 3, 4, 6, 7, S1–S3, S5, S6, and S8) or number of cells (Figures 5 and S7), all of which have been specified in Figures.